April 24, 2023

The *Toxoplasma* monocarboxylate transporters are involved in the metabolism within the apicoplast and are linked to parasite survival

Hui Dong[a,b,1], Kai He[a,b,1], Jiong Yang[c,1], Wen-Bin Zheng[d], De-Hua Lai[c], Jing Liu[a,b], Hui-Yong Ding[a,b], Rui-Bin Wu[a,b], Kevin M. Brown[e], Geoff Hide[f], Zhao-Rong Lun[c], Xing-Quan Zhu[d], Shaojun Long[a,b,#]

[a]National Key Laboratory of Veterinary Public Health Security, College of Veterinary Medicine, China Agricultural University, Beijing 100193, China

[b]National Animal Protozoa Laboratory and School of Veterinary Medicine, China Agricultural University, Beijing 100193, China

[c]State Key Laboratory of Biocontrol, School of Life Sciences, Sun Yat-Sen University, Guangzhou 510275, China

[d]College of Veterinary Medicine, Shanxi Agricultural University, Taigu 030801, Shanxi Province, China

[e]Department of Microbiology and Immunology, University of Oklahoma Health Sciences Center, Oklahoma City, Oklahoma, USA

[f]Biomedical Research and Innovation Centre and Environmental Research and Innovation Centre, School of Science, Engineering and Environment, University of Salford, Salford, M5 4WT, UK

[1]These authors contributed equally to the work

[#]To whom correspondence may be addressed:

Shaojun Long, LongS2018@163.com

Abstract

The apicoplast is a four-membrane plastid found in the apicomplexans, which harbors biosynthesis and organelle housekeeping activities in the matrix. However, the mechanism driving the flux of metabolites, in and out, remains unknown. Here we used TurboID and genome engineering to identify apicoplast transporters in *Toxoplasma gondii*. Among the many novel transporters, we show that one pair of apicomplexan monocarboxylate transporters (AMTs) appears to be evolved from the putative host cell that engulfed a red alga. Protein depletion showed that AMT1 and AMT2 are critical for parasite growth. Metabolite analyses supported the notion that AMT1 and AMT2 are associated with biosynthesis of isoprenoids and fatty acids. However, stronger phenotypic defects were observed for AMT2, including in the inability to establish *T. gondii* parasite virulence in mice. This study clarifies, significantly, the mystery of apicoplast transporter composition and reveals the importance of the pair of AMTs in maintaining the apicoplast activity in apicomplexans.

Key words

Apicomplexans, *Toxoplasma gondii*, Apicoplast, TurboID, Transmembrane Proteins, Transporters, Monocarboxylate Transporters, Isoprenoid Biosynthesis, Fatty acids.

Introduction

The phylum Apicomplexa encompasses thousands of intracellular parasites, including *Plasmodium*. spp., the notorious agent of malaria, and *Toxoplasma gondii*, the highly successful parasite that infects almost all warm-blooded animals and humans (Plattner and Soldati-Favre, 2008). It is believed that apicomplexan evolution included two key independent, and sequential, endosymbiotic events, finally leading to the common ancestor of the chromalveolates (e.g. alveolates, heterokonts, oomycetes and Cryptomonads) (Cavalier-Smith, 1999; Gould et al., 2008; Janouskovec et al., 2010). This ancestor eventually gave rise to the apicomplexans, most of which still contain, a secondary non-photosynthetic plastid, the apicoplast (McFadden and Yeh, 2017; Obornik et al., 2009; Salomaki and Kolisko, 2019). Therefore, the apicoplast membranes have evolved from the red algal plastid, the algal plasma membrane and the host endomembrane when counting from the innermost to outermost membranes of the apicoplast (Gould et al., 2008; McFadden and Yeh, 2017). This heavily compartmentalized feature poses great challenges for metabolic integration of the organelle within the parasites and, in particular, the transport of metabolites across these membrane systems.

The apicoplast houses essential biosynthetic pathways, which include the fatty acid synthesis type II (FASII), methylerythritol phosphate (MEP) pathways, Fe-S cluster and (partial) heme biosynthesis pathway (Fata and Rabuzzi, 1988; Kloehn et al., 2021; Krishnan et al., 2020; Ralph et al., 2004; Tjhin et al., 2020). They are able to make critical components of fatty acids and isoprenoid precursors, for the parasites in *T. gondii* and *Plasmodium falciparum* (McFadden and Yeh, 2017; Ramakrishnan et al., 2012; Striepen, 2011; Vaughan et al., 2009; Yeh and DeRisi, 2011). Moreover, the apicoplast maintains housekeeping activities for genome replication, transcription and translation (Low et al., 2018; McFadden and Roos, 1999). Accordingly, it requires adequate supplies of carbon molecules, energy, reducing equivalents, cofactors, amino acids, nucleotides as well as inorganic ions, to feed the biosynthetic pathways and plastid maintenance activities in the matrix (Kloehn et al., 2021; McFadden and

Yeh, 2017; Ralph et al., 2004). However, compared to plant plastids, the nature of the channels and transporters in the apicoplast remains obscure.

The apicoplast biosynthetic pathways were characterized through a homology/bipartite signal-based approach (Foth et al., 2003; Ralph et al., 2004). A similar approach was utilized to identify phosphate translocators in *T. gondii* (i.e. *Tg*APT1) and *P. falciparum* (i.e. *Pfi*TPT and *Pfo*TPT), and a two-pore channel TPC in *T. gondii*. These transporters are capable of supplying phosphorylated carbons, (Brooks et al., 2010; Fleige et al., 2007; Karnataki et al., 2007; Lim et al., 2010; Mullin et al., 2006), and calcium to the apicoplast (Li et al., 2021). It was proposed that an early step in the endosymbiotic event was to integrate transporters that exchange metabolites across the membranes (Cavalier-Smith, 2000; Weber et al., 2006). Consistent with that, studies demonstrated that 57-58% of the chloroplast transporters have an origin in the putative host cell in the first endosymbiosis while 20-30% are from bacteria (Karkar et al., 2015; Tyra et al., 2007). It is plausible that a complex transporting system was produced in the evolution of the secondary plastid (i.e. the apicoplast).

Recent studies suggested that we still do not know the major source of pyruvate required for the biosynthesis pathways in the apicoplast of *T. gondii* and *P. falciparum* (Swift et al., 2020; Xia et al., 2019). Thereafter, identifying the apicoplast transporter composition and their functions is critical for an understanding of how these transporters evolved and how the organelle maintains its metabolic and housekeeping activities. In this study, we utilized the apicomplexan model organism *T. gondii* to screen apicoplast membrane proteins, identified from available computational and proteomic information (Barylyuk et al., 2020; Boucher et al., 2018) and from our APT1-TurboID proximity proteomic candidates, and discovered several novel apicoplast transporters. Among the many transporter candidates, one pair of monocarboxylate transporters (AMTs) appeared to have evolved from the putative host cell involved in the evolution of the secondary plastid. Detailed analyses support

115 association of the AMTs with the apicoplast biosynthesis pathways likely by supplying
116 the pathways with substrates. This study opens up the possibilities of tackling difficult
117 questions of substrate transport and especially for the pair of monocarboxylate
118 transporters in *T. gondii* and in other members of this phylum of deadly parasites.

119

120 **Results**

121 **Discovery of novel transporters in the apicoplast of *T. gondii***

122 To identify apicoplast transporter proteins in *T. gondii*, we first analyzed candidates
123 identified in recent studies using combined proteomic and computational analyses in *T.*
124 *gondii* and *P. falciparum* (Barylyuk et al., 2020; Boucher et al., 2018). The hyperplexed
125 localization of organelle proteins (hyperLOPIT) assigned 129 proteins to the
126 apicoplast (Barylyuk et al., 2020), of which three proteins were likely transporters, i.e.
127 APT1 (Transmembrane Domain, TMD=6), one major facilitator superfamily (MFS)
128 transporter (TGME49_309580) (HAP1, hypothetical apicoplast protein 1) and one
129 hypothetical protein (TGME49_267690) (HAP2) (Table S1). We also mined an
130 apicoplast proteomic dataset obtained by ACP-BioID in *P. falciparum* (Boucher et al.,
131 2018), which reported 16 TMD≥6 protein candidates, and two additional candidates
132 annotated as ABC transporters (TMD<6). We identified the orthologues in *T. gondii*
133 using the *P. falciparum* candidates (Boucher et al., 2018; Sayers et al., 2018),
134 resulting in 8 candidates in *T. gondii*. They were temporarily named as HAP3-9 (Table
135 S1). Taken together, these datasets provided only limited numbers of candidate
136 transporters.

137 To better define the repertoire of apicoplast transporters, we employed a biotin
138 proximity labeling strategy that is useful for defining organelle proteomes. A
139 promiscuous biotin ligase tag called TurboID was endogenously fused with APT1,
140 using a CRISPR approach (Table S2-4) (Branon et al., 2018; Brooks et al., 2010;
141 Long et al., 2018). The apicoplast Acetyl-CoA carboxylase 1 (ACC1) is a strongly

142 biotinylated protein (Zuther et al., 1999), which might provide a clear and strong
143 streptavidin labeling at the apicoplast (Figure 1A). Though the streptavidin signal and
144 the protein itself were slightly diffused (Karnataki et al., 2007), APT1 was reported to
145 mainly localize to four of the apicoplast membranes (Karnataki et al., 2007). Many
146 additional bands present on the APT1-TurboID lane were likely to be the apicoplast
147 proteins (Figure 1B). The resultant mass-spectrometry datasets (N=3 for each)
148 (Dataset S1) were analyzed by comparing the APT1-fusion to the parental line (Figure
149 1C and Table S5). This analysis showed that APT1 itself has the highest *p*-value
150 associated with its enrichment in the TurboID line, as would be expected for a bait
151 protein. The TMD candidates (TMD≥6 and 2≤TMD<6) were evenly distributed on the
152 volcano map plotted by fold changes against *p*-values in a similar pattern to the
153 distribution of known apicoplast proteins (Figure 1C and Table S6). These features
154 suggested that APT1-TurboID had enriched apicoplast proteins. Thereafter, we
155 compiled a list of the hits in order of TMD numbers, and selected all transporter
156 candidates (including carriers) and hypothetical proteins (TMD≥6) as candidates
157 (Table S7). These candidates were merged with the previously described ones
158 (HAP1-9) and temporarily named as HAP10-50 (Table S8).

159 After the above candidate selections, as described in our workflow (Figure1D), we
160 compiled a list of 50 candidates (HAP1-50) for endogenous tagging and IFA analysis
161 in *T. gondii*. We successfully generated endogenous HAP-6Ty fusion lines (46 HAPs)
162 using a CRISPR-Cas9 tagging approach (Figure S1A and Tables S2-4), as described
163 in our previous study (Long et al., 2017b). Indirect fluorescence assay (IFA) showed
164 that many HAP-6Ty fusions were localized to foci inside the parasites, resembling the
165 position of the apicoplast location (Figure S1A), whereas some candidates were likely
166 to be in the cytosolic vesicles (e.g. HAP13, HAP30, HAP35), the apical region (e.g.
167 HAP19) or other structures (e.g. HAP22) (Figure S1B). Further analysis was
168 performed by co-localization of the fusions with an apicoplast marker ACP, which
169 showed that many of the foci had no or only partial co-localization with ACP (Figure

170 S2A). However, strict analyses clearly identified 15 HAP fusions that were almost
171 perfectly co-localized with ACP (Figure 1E).

172 Of the 15 novel apicoplast membrane proteins, we identified in *T. gondii* that 12
173 proteins are annotated as putative transporters or carriers in TOXODB, and 3 are
174 annotated as hypothetical proteins (TMD≥6) (Figure 1F and Table S9). These novel
175 proteins included 1 from hyperLOPIT, 3 from ACP-BirA and 14 from our APT1-TurboID
176 (Figure 1G), among which three of these proteins shared between the APT1-TurboID
177 and the combinations of hyperLOPIT and ACP-BirA (Figure 1H). Collectively, TurboID
178 proved to be a reasonably robust approach for the identification of putative apicoplast
179 transporters.

180 **Novel transporters are mostly conserved in the Apicomplexa**

181 To determine if the apicoplast transporters we identified in *T. gondii* are conserved in
182 the Apicomplexa, we searched for orthologues of these novel proteins in different
183 species, as shown in Fig. 2A-B. The chromalveolate hypothesis proposed a plastid
184 origin in a common ancestor of a single red alga, which unites the Alveolates with the
185 chromists (Cavalier-Smith, 1999). We identified orthologues in species belong to the
186 taxa using a powerful Hidden Markov Model (HMM) profiling strategy. The best hits
187 (the cutoff E-value: 1x10-7) remained on the list of resultant orthologues in these
188 species, which were then used for conservation analyses in the ComplexHeatmap
189 package in R (v4.2.0) (Gu et al., 2016) (Table S10, which contains the hits with
190 E-values). The conservation heatmap showed that proteins with conserved transport
191 domains (HAP1, 3, 4, 9, 10, 28, 33, 34, 41 and 50) are mostly conserved in the
192 Apicomplexa (Figure 2A), including the Gregarina and *Cryptosporidium* that have lost
193 the apicoplast. Further analysis revealed that most orthologues with the exception of
194 HAP3 and HAP4, can be identified in green algae, red algae and plants (Figure 2B).
195 As the red alga is considered to have given rise to the ancestor of the secondary
196 plastid (Gould et al., 2008; Janouskovec et al., 2010), the results thus indicated that

those transporters were possibly derived from the red alga. However, further analysis would be required to clarify their origins, as shown for chloroplastid transporters (Karkar et al., 2015).

AMT1 and AMT2 might have critical roles in metabolic integration of the apicoplast

Several transporters, such as HAP1, 3, 4, and 34 and 50, are predicted to be essential in *T. gondii* and in *P. falciparum* (Figure 2A-B, and Table S9 contains the *P. falciparum* orthologues with fitness scores) (Sidik et al., 2016; Zhang et al., 2018). The analyses with InterProScan showed that three of these transporters (HAP1, 3 and 4) belong to the major facilitator superfamily (MFS) (Figure S2B). The MFS is a large family of transporter capable of transporting small solutes in response to chemiosmotic ion gradients (Pao et al., 1998; Walmsley et al., 1998). These MFS transporters contain a pair of monocarboxylate transporter (MCT) with 11-12 TMDs (Figure S2C). The MCTs play essential roles in the transport of nutrients, such as pyruvate, lactate, amino acids and so on, in the plasma membrane of human cells (Felmlee et al., 2020). These features attracted our intense attention, and thus named the MCTs as **A**picoplast **M**onocarboxylate **T**ransporters (AMTs, AMT1 for HAP3, TGGT1_233540; AMT2 for HAP4, TGGT1_297245).

We noticed that these two transporters are absent in red algae, green algae and plants (Figure 2B). This observation is in contrast to APT1, which was identifiable in these primary plastid-containing taxa (e.g. plants) but not in cyanobacteria (Figure 2B). Evolution and phylogenetic analyses suggested that the plant orthologues of APT1 are derived from a putative host cell that previously engulfed a cyanobacteria (Knappe et al., 2003; Weber et al., 2006). The pair of AMTs appears similar to the APT1 situation, indicating that they were possibly derived from the heterotrophic protist – the putative host cell - that previously engulfed a red alga. The AMTs were identifiable in the photosynthetic relative (e.g. *Chromera velia*) of the apicomplexans, and a distant

224 relative taxa of Oomycetes (Figure 2A), indicating a broader conservation in these
225 species. We further analyzed orthologues in selected species of apicomplexans, and
226 found that most species contain at least two identifiable orthologues, including
227 *Crytosporidium spp*. (Table S11). Collectively, the pair of AMTs are likely to have
228 critical roles in metabolic integration of the endosymbiont in the parasite cytosol
229 during evolution.

230 **AMT1 and AMT2 are essential for the parasites**

231 The confocal imaging showed that AMT1-6Ty was almost perfectly co-localized with
232 AMT2-6HA (Figure S3A), suggesting that the putative transporters are highly likely to
233 be localized at the apicoplast membranes. In support of this model, immuno-Electron
234 Microscopy (immuno-EM) provided a further piece of evidence, supporting the
235 membrane localization of AMT1 and AMT2 (Figure S3B). Due to the complexity of the
236 apicoplast membranes, and heterogeneity of immunolabeling, the precise topology of
237 AMT1 and AMT2 within the apicoplast membranes merits future investigation. To
238 analyze the physiological functions of the AMTs, we generated the conditional
239 knockdown lines using an IAA-inducible degron (AID) system in *T. gondii* (Brown et al.,
240 2017; Long et al., 2017b). The CRISPR-Cas9 genome editing approach was utilized
241 to specifically fuse the AID-6Ty at the 3'-terminus of the genes in the IAA receptor
242 (TIR1) expressing line RH TIR1 (Figure S4A). To conditionally study both proteins
243 together, we fused AMT2 with AID-3HA at the 3'-terminus in the background of
244 AMT1-AID-6Ty, creating a double knockdown line AMT1-AID-6Ty/AMT2-AID-3HA
245 (dKD). Correct integration of the AID fragments was confirmed by diagnostic PCR as
246 demonstrated in the schematic diagram (Figure S4A-B). As expected, the AID fusions
247 were efficiently and stably depleted in IAA treatments for 3-36 hours, as shown on
248 Western blots (Figure 3A). It was noteworthy that Western blots detected two bands in
249 the single and double AID fusion lines, which appeared to be the precursor and
250 mature forms of AMT1 and AMT2 (Figure 3A). So far, several membrane proteins
251 have been identified in the apicoplast of *T. gondii*, four of which were observed to be

252 processed (FtsH1, TiC20, ATrx1 and TPC) (DeRocher et al., 2008; Karnataki et al.,
253 2007; Karnataki et al., 2009; van Dooren et al., 2008). Yet, at least ATrx1 and FtsH1
254 lack canonical signal peptides. However, in *P. falciparum,* PfiTPT is processed and
255 cleaved, while PfoTPT is unprocessed due to its absence of a signal peptide (Mullin et
256 al., 2006). It appear that processing and topology of ATMs are complex and
257 unpredictable in *T. gondii*. Further analysis by IFA showed that the AID fusions were
258 correctly localized to the apicoplast and were depleted within 24 hours of IAA
259 treatment (Figure 3B and Figure S4C); however, the parasite bodies were
260 morphologically normal. To assess lytic growth of the AID lines, we assayed plaque
261 formation of the AID parasites on host cell monolayers for 7 days. We observed that
262 the AID lines grown in IAA did not form discernible plaques (Figure 3C), which was
263 supported by further analysis of the plaque numbers and areas (Figure 3D-E). In
264 summary, the AMTs are potentially essential for *in vitro* parasite growth.

265 We wondered if parasite replication contributed to the plaque defects. The parasites
266 were grown in IAA for 24 hours, followed by scraping, purification and re-infection for
267 the assay in the 2nd 24 hours and 3rd 24 hours. Using IFA analysis of the parasites, we
268 observed that parasite replication was significantly affected in the first 24 hours of
269 growth and became worse in the following cycles of 24 hours, especially the 3rd 24
270 hour period (Figure 3F). These results suggested that depletion of the transporters
271 caused strong growth defects and delayed death of the parasites. We wondered if
272 depletion of the proteins could cause loss or breakdown of the apicoplast, as reported
273 previously for many apicoplast proteins (Kennedy et al., 2019b). ACP, an apicoplast
274 marker, was used to test the apicoplast status (Waller et al., 1998). We observed that
275 ACP partially diffused in the cytosol of intracellular parasites grown in IAA for 24 hours
276 (Figure S5A), whereas it completely diffused in the cytosol of extracellular parasites
277 that had grown in IAA for 24 hours (Figure S5B). This observation suggested swelling
278 or breakdown of the apicoplast in the intracellular or extracellular parasites depleted
279 with the AMTs, respectively. Detailed analysis of the phenotypes showed that the ACP

280 diffusion gradually increased while comparing the three cycles for the same AID line in
281 both the intracellular and extracellular parasites (Figure 3G-H). However, it was as low
282 as ~30% in AMT1-AID, compared to those (60-70%) in AMT2-AID and dKD (Figure
283 3G-H). These results suggested that depletion of AMT2-AID resulted in much more
284 severe defects (swelling or breakdown) of the apicoplast than that of AMT1-AID, and
285 further depletion of AMT1-AID had no further effect.

286 **Depletion of the proteins resulted in defects in metabolic pathways**

287 Based on the evolutionary predictions and features of monocarboxylate transporters,
288 we suspected that the AMTs might be involved in transport of substrates, such as
289 pyruvate, lactate, amino acids, as reported for human MCTs (Felmlee et al., 2020). As
290 such, depletion of AMT1 and AMT2 would result in reduced levels of the metabolites
291 of IPP and fatty acids in *T. gondii*. We first designed experiments to examine the
292 possible defect of IPP synthesis in the AID lines upon induction, by assaying the
293 capabilities of endocytic trafficking of GFP vesicles to the vacuolar compartment (VAC)
294 (Dou et al., 2014). Our recent data showed that GFP transport to the VAC following its
295 uptake from host cell cytosol is dependent on protein prenylation of Rab1B and
296 YKT6.1 (unpublished data). These proteins are modified at the C-terminal motif by
297 isoprenoids, the synthesis of which could be specifically inhibited by atorvastatin at
298 the host cells and by zoledronate in the parasite (Li et al., 2013), as demonstrated in a
299 schematic and in positive experiments (TIR1 with two drugs at IC50 concentrations)
300 with reduced GFP transport (Figure 4A-B). Therefore, measuring the endocytic
301 trafficking of GFP vesicles in parasites in the absence/presence of atorvastatin could
302 reflect levels of protein prenylation, and thus levels of IPP synthesis in the parasites.
303 We then assayed the TIR1 and AID lines by growing them in GFP expressing HFF
304 monolayers, where experimental groups were controlled by absence/presence of
305 atorvastatin and IAA (Figure 4B), and where LHVS was added to avoid degradation of
306 GFP in the VAC. Following endocytosis of GFP vesicles by the micropore (manuscript
307 in press), GFP vesicles were successfully transported to and accumulated in the VAC

308 of TIR without IAA, with a high percentage (>20%) of parasites containing GFP foci
309 (Figure 4B). In contrast, the GFP vesicles diffused through the cytosol, and were
310 unable to accumulate at the VAC in the AID parasites grown in IAA with the
311 absence/presence of atorvastatin, as shown by significantly reduced percentages
312 (~8%) of the parasites in the AID lines induced for 12 hours (Figure 4B). We further
313 tested Rab1B stability in the AMT-AID lines grown in IAA for 12 hours, which showed
314 a strong defect of reduced protein abundance of Rab1B by scoring of parasites with
315 normal or abnormal level of Rab1B using an IFA approach (Figure S5C). This
316 phenotype was observed in parasites with a reduced supply of isoprenoids by drug
317 inhibition or knockdown of prenyl-transferase GGT-2 (unpublished data). These
318 results altogether thus suggested that the IPP synthesis is significantly decreased in
319 the AID lines depleted with the transporters. However, it was noteworthy that parasites
320 depleted with AMT1-AID and AMT2-AID had similar levels of reduced GFP transport
321 and parasites with reduced protein abundance of Rab1B at the 12 hours of IAA
322 induction, suggesting that depletions of AMT1 and AMT2 resulted in similar levels of
323 IPP reduction in parasites.

324 Our results in *T. gondii* reported a physiological effect that was observed in *P.*
325 *falciparum*, where inhibition of the MEP pathway by fosmidomycin caused disruption
326 of hemoglobin transport (Howe et al., 2013; Kennedy et al., 2019a). Herein, our
327 results underscored the importance of the transporters for supporting the MEP
328 pathway in the apicoplast. This was further manifested by a reduced level of
329 mitochondrial membrane potential detected by mitotracker red in the AMT1-AID or
330 AMT2-AID lines grown in IAA for 24 hours (Figure S5D). IPP is the precursor for
331 synthesis of ubiquinone, an essential electron carrier required for electron transport in
332 the mitochondria (Kennedy et al., 2019b; Sleda et al., 2022). The reduced
333 mitochondrial potential was also observed in the parasites depleted with APT1
334 (Brooks et al., 2010). Thus, the reduced mitochondrial membrane potential provided
335 another piece of evidence supporting the notion of defective IPP synthesis in

336 parasites depleted with the transporters.

337 We further examined activity of the FASII pathway in the TIR1 and AID lines grown in
338 IAA for 18 hours, by testing metabolites (e.g. FA) in the parasites using untargeted
339 metabolomics (GCMS and LCMS). The metabolomics detected 66 metabolites in total
340 in these lines (Dataset S2). After analyses using Dunnette's multiple comparison
341 methods, 15, 23, and 34 differential metabolites were identified in the parasite groups
342 depleted with either AMT1-AID, AMT2-AID or both (dKD) (Table S12), in comparison
343 with TIR1. Interestingly, three AID lines shared 13 differential metabolites (Figure 4C).
344 The shared metabolites included fatty acids and lipids, such as myristic acid (C14 fatty
345 acid), palmitoleic acid (C16 fatty acid), trans-oleic acid (C18 fatty acid) and
346 phospholipids containing C14 and C18 fatty acids (Figure 4D). These results were
347 consistent with previous studies where inactivated FASII proteins led to reduced
348 synthesis of fatty acids up to 18 carbons long, and exogenous additions of the C14
349 and C16 fatty acids could complement growth defects (Liang et al., 2020;
350 Ramakrishnan et al., 2012). These results suggested that depletion of the
351 transporters significantly impaired FASII activity. In contrast to the same level of
352 reduced endocytic trafficking of GFP vesicles in the AID lines, reduction in levels of
353 the C14, C16 and C18 fatty acids was much stronger and more significant in
354 AMT2-AID and dKD than in AMT1-AID (Figure 4D), supporting the notion of a
355 stronger impairment of the FASII pathway in parasites depleted with AMT2-AID.

356 Intriguingly, the metabolomics also identified metabolites related to the TCA cycle,
357 such as gamma-aminobutyric acid (GABA), glutamic acid, and succinic acid (Figure
358 4E), which were shared among three of the AID lines. This would likely result from
359 defective membrane potential caused by a reduced supply of IPP for synthesis of
360 ubiquinone, as described above, or synthesis of heme that requires co-operation
361 between the mitochondrion and the apicoplast (Harding et al., 2020). Another two
362 metabolites, creatine and lactic acid, were likely associated with reduced metabolic
363 levels in the parasites (Figure 4E).The untargeted metabolomics tends to identify

364 differential metabolites by comparing the AID to TIR1 lines. Pyruvate was not
365 identified, as it is actually a product of glycolysis in the cytosol. Collectively, the
366 transporters are expectedly associated with the MEP and FASII pathways, to support
367 synthesis of IPP and FA in the apicoplast.

368 **Depletion of AMT2 affects stability of ACC1**

369 Depletion of AMT2 resulted in stronger defects on ACP diffusion and synthesis of fatty
370 acids, suggesting a more important role of AMT2 in the apicoplast. To find out the
371 reason for this, we first examined the protein level of one AMT (fused with 6HA) in
372 another AMT's AID-Ty line, thus assuring no reciprocal effect on protein level. After
373 IAA induction for 36 hours, we did not see obvious changes to protein levels in the
374 6HA fusions in the AID-Ty lines on western blots and IFA (Figure S6A-B). Considering
375 a MCT could transport biotin in mammalian cells (Daberkow et al., 2003), we
376 wondered if AMT2 was able to transport biotin for activation of acetyl-CoA carboxylase
377 ACC1, which is a key enzyme in FASII (Zuther et al., 1999). ACC1 was endogenously
378 fused with 6HA in the AID lines by a CRISPR approach. Upon protein depletion in IAA
379 for 36 hours, ACC1 was found to be gone only in the AMT2-AID parasites, but not in
380 the AMT1-AID parasites, as demonstrated by Western blots (Figure S6C). Further
381 analysis showed that ACC1 was gone in some parasites within a single vacuole in the
382 AMT2-AID-depleted parasites, where ACP was clearly stained with a slight diffusion
383 (Figure 6D). Based on the presence or absence of ACC1 in parasites of the vacuoles,
384 we can classify the vacuoles into three types - all parasites without ACC1 (type 1),
385 one parasite (type 2) or two parasites (type 3) with ACC1 (Figure S6E). The
386 quantification assay showed that only ~40% of the vacuoles contained one or two
387 parasites with ACC1 signal (type 2 and type 3) (Figure S6F). However, ACC1 in those
388 parasites was still biotinylated, as shown in streptavidin stains (Figure S6G).
389 Collectively, AMT2 is associated with stability of ACC1 in a way, as yet, unknown, but
390 unrelated with biotin availability in the apicoplast.

391 **AMT2 is essential to parasite growth in mice**

392 We next examined the *in vivo* growth of the AID parasites in mice administered with
393 IAA. Prior to the mice assay, we attempted to gain further information about the
394 ultra-structures of the apicoplast upon depletion of the AMTs. The transmission
395 electron microscopy (TEM) demonstrated that the four membranes surrounding the
396 apicoplast remained visible, but were loosened, and the interior of the organelle
397 appeared less dense and even electron lucent in the AID parasites, which had been
398 induced for 24 hours in comparison with the TIR1 parasites (Figure 5A). We further
399 quantified the apicoplasts with a reduced electron density in the AID parasites induced
400 for 12, 24 and 36 hours vs the TIR1 in IAA for 36 hours, by examining 300 parasites in
401 each time point. This examination showed that the apicoplast numbers identified by
402 TEM dropped in the AMT1-AID parasites, when induced for 24 hours and 36 hours,
403 and the numbers dropped by much greater levels in the AMT2-AID parasites,
404 following 12 hours of IAA induction (Figure 5B). Notably, the apicoplast was identified
405 only 3 times in the AMT2-AID parasites at 36 hours induction. Accordingly, the
406 percentage of the abnormal apicoplast increased for both of the AID lines. In contrast,
407 depletion of AMT2-AID resulted in much higher levels of abnormal apicoplasts at the
408 three induction time points, compared to those in parasites depleted with AMT1-AID
409 (Figure 5B). These results suggested that depletion of AMT1 caused modest loss of
410 the apicoplast, yet the AMT2 depletion appeared to have a greater effect on the
411 apicoplast loss.
412
413 The parental line TIR1 and its derivative lines (AMT1-AID, AMT2-AID and dKD) were
414 then used to intraperitoneally infect mice, at 100 parasites per mouse, followed by
415 administering the mice orally and intraperitoneally with IAA in a solution on a daily
416 basis. Those mice infected with TIR1 succumbed to lethal toxoplasmosis by day 10
417 post infection (Figure 5C). Conversely, the IAA treatment ultimately prevented acute
418 virulence caused by the parasite lines with the AMT2 depletion (i.e. AMT2-AID and

419 dKD), and it postponed mouse death by the AMT1-AID depletion. We next tested sera
420 extracted from the surviving mice (which were infected by AMT2-AID) by performing
421 IFA on *T. gondii* parasites. The IFA showed that the mouse sera clearly recognized
422 proteins of the parasitophorous vacuoles of the parasites (Figure S7A). We also
423 further analyzed the efficacy of protein degradation of the AMT1-AID fusions in mice,
424 by treatment with or without IAA for 24 hours after 5 days of growth, as illustrated in
425 Figure S7B. It was clear that AMT1-AID was efficiently degraded in mice by the
426 treatment of IAA in only 24 hours (Figure S7B). These results demonstrated that the
427 mice infection assays were robust. However, the strong growth conferred by AMT1
428 depletion in parasites in cell culture surprisingly resulted in only reduced parasite
429 virulence in mice. We assume that this discrepancy is related to the relatively modest
430 defects, such as the ACP diffusion/apicoplast abnormality (revealed by TEM)/FASII
431 activity, as observed in the AMT1-depleted parasites. Thus, the remaining apicoplast
432 is still functionally generating adequate amount of metabolites, allowing the parasites
433 to survive in mice. However, the discrepancy is possibly associated with transport
434 capability of substrates by AMT1 and AMT2. Though this does not perfectly explain
435 the discrepancy, phenotypes in AMT1-depleted parasites argue for this possibility.
436 Collectively, AMT2 was obviously essential for establishing *T. gondii* infection and
437 growth in mice.
438
439 **Discussion**
440 Most of the apicomplexan parasites, such as *T. gondii* and *Plasmodium spp*., harbor a
441 vestigial plastid, which undergoes several fitness-conferring or essential metabolic
442 pathways in the matrix (Kloehn et al., 2021; Lim and McFadden, 2010). However, the
443 transporters that are responsible for exchanging metabolites between the apicoplast
444 and the parasite remain elusive, due to difficulties in identification of those
445 transporters in the multiple membranes that surround the organelle. Here we fully
446 exploited the currently available data, and the high-efficiency of proximity biotin

447 labeling and CRISPR-Cas9 tagging approaches in the model apicomplexan *T. gondii*,
448 and discovered several novel transporters in the apicoplast. Among those putative
449 transporters, most of them appear to be derived from the endosymbiont (i.e. a red
450 alga) in evolution of the secondary plastid, and only the pair of monocarboxylate
451 transporters AMT1 and AMT2 is likely to be derived from the putative host cell that
452 originally engulfed the endosymbiont. Protein depletion of the AMT1 and AMT2, using
453 a highly efficient technique the TIR1-AID system, resulted in defects of plaque
454 formation *in vitro*, ACP diffusion/apicoplast loss, and biosynthetic pathways of the
455 MEP and FASII. However, depletion of AMT2 clearly caused stronger defects
456 including ACP diffusion/apicoplast loss, FASII products fatty acids, ACC1 stability and
457 removed mouse virulence. These results indicate that complex transporting functions
458 are likely to exist in the apicoplast for AMT1 and AMT2.
459
460 Recent studies have highlighted the difficulty in identifying apicoplast transporters,
461 because of strong backgrounds in the proteomics (Boucher et al., 2018; Sayers et al.,
462 2018). This remained true for our proximity proteomics from APT1-TurboID.
463 Fortunately, our focused screening leveraged high efficiency by genomic editing in *T.*
464 *gondii,* yielding positive results for 12 putative transporters. These novel transporters
465 provided an important resource for evolution and functional analyses. Their
466 conservation, including in plastid-deficient taxa, i.e. Gregarina and Cryptosporidia,
467 indicates that these proteins were relics of the former plastid in evolution via
468 endosymbiont gene transfers (EGT) (Gould et al., 2008). Studies suggested that the
469 metabolic integration of the primary plastid (e.g. chloroplast) was mainly driven by
470 targeting transporters from a heterotrophic protist - the host cell, but not from the
471 endosymbiont - cyanobacteria (Karkar et al., 2015; Tyra et al., 2007). However, our
472 preliminary study in evolution indicated that most novel transporters were likely to be
473 derived from the endosymbiont. In sharp contrast, the pair of monocarboxylate
474 transporters (AMT1 and AMT2) may have an origin in a heterotrophic protist – the

475 putative host cell. This observation therefore provides a perspective that the pair of
476 AMTs may play critical roles in metabolic integration of the algal endosymbiont into the
477 parasites.
478
479 Our immuno-EM and confocal imaging provided a strong support for the membrane
480 localization of the pair of transporters AMT1 and AMT2 in the apicoplast, indicating
481 that the AMTs are likely to transport substrates in the membranes. We observed that
482 the AMTs are clearly processed, though they lack signal peptides. Concerning the
483 processing and targeting, apicoplast membrane proteins in *T. gondii* appear to be
484 more complex than those in *P. falciparum*, by comparison to PfiTPT and PfoTPT
485 (Mullin et al., 2006). Our phenotypic analysis showed that depletion of the
486 transporters AMT1 and AMT2 caused strong defects on plaque formation and parasite
487 replication, suggesting that both transporters are critical on the apicoplast membranes.
488 However, we observed disparate degrees of phenotypic disruption in the
489 AMT1-depleted and AMT2-depleted parasites. Depletion of AMT2 always caused
490 stronger defects in ACP diffusion, FASII fatty acids, apicoplast loss and mouse
491 virulence. AMT2 is additionally associated with loss of ACC1, a key enzyme for FASII,
492 found in the majority of parasites in a vacuole, likely providing another piece of
493 evidence to explain the greater phenotypic defects. Several attempts to delete ACC1
494 failed in our study, supporting a critical role of ACC1 in the FASII process. Genetic
495 studies suggest that depletion of FASII enzymes led to loss of apicoplast (Krishnan et
496 al., 2020; Liang et al., 2020). Thus, the observation of ACC1 loss support stronger
497 phenotypes in AMT2-AID depleted parasites. In addition, depletion of the AMTs
498 caused an initially gradual defect, but then a much more focused sharper defect in
499 parasite replication in the 3rd 24 hours and showed a delayed death phenotype.
500 Previous studies showed that parasite replication exhibited gradual deceases upon
501 depletion of TPC and APT1 by utilization of a low efficient knockdown strategy - the
502 tetracyclin-inducible system (TATi) (Brooks et al., 2010; Li et al., 2021). It is unknown

503 that the TATi system would mask the growth phenotype, yet, the AMT depletion
504 appeared to have such a sharper change in the third cycle (24 hours in a growth
505 cycle). Collectively, the AMTs are critical to parasites, yet AMT2 is more important to
506 the apicoplast membrane function.
507
508 Based on knowledge of MCTs (Felmlee et al., 2020), the pair of AMTs is likely to
509 transport pyruvate, lactate, amino acids and other substrates. We thus suspect that
510 AMT1 and AMT2 might be associated with transporting pyruvate and amino acids,
511 since these are essential for the apicoplast metabolism. Pyruvate is the central
512 metabolite that connects many metabolic pathways in living organisms. It must be
513 imported into organelles for specific metabolic pathways, as suggested with pyruvate
514 import by the NHD1/Bass2-protein coupling function in the chloroplast of C4 plants,
515 and by the mitochondrial pyruvate carrier MPC (Bricker et al., 2012; Furumoto, 2016;
516 Furumoto et al., 2011; Gasperotti et al., 2020; Herzig et al., 2012). In *T. gondii*, and *P.*
517 *falciparum*, studies have suggested that the major pyruvate source has still not been
518 established (Niu et al., 2022; Swift et al., 2020; Xia et al., 2019). The possible role on
519 pyruvate import by the AMTs could provide a good explanation for the defects on MEP
520 and FASII pathways, especially on the reduced levels of IPP synthesis resulting from
521 the protein depletion. We attempted to define this possible function of the AMTs by a
522 pyruvate sensor PyronicSF in the parasite (Arce-Molina et al., 2020), and by a
523 complementation of an *Escherichia. coli* knockout strain that is deficient in pyruvate
524 import (a generous gift from Prof. Kirsten Jung) (Gasperotti et al., 2020); however,
525 several attempts with these approaches were not successful for detailed examination
526 of pyruvate import capability either in the parasite or in the *E. coli* strain.
527
528 Our work successfully identifies several novel apicoplast transporters, thus greatly
529 unravelling the mystery of the apicoplast membrane composition and opening up the
530 possibilities to tackle difficult questions about metabolite transport in the

531 apicomplexans. The most intriguingly findings in this study are the identification of the
532 pair of monocarboxylate transporters AMT1 and AMT2, which are likely derived from
533 the putative host cell that engulfed a red algal during the evolution of this group of
534 parasites. Metabolic analysis together with other phenotypic analyses supported the
535 notion that the pair of AMTs is associated with the MEP and FASII biosynthesis
536 pathways. However, though both transporters belong to the MCTs, the phenotypic
537 defects differ greatly, supporting a complex function for AMT2 in the apicoplast.
538 Collectively, the monocarboxylate transporters are likely to control similar essential
539 processes in related protists.
540
541 Limitations of This Study
542 This study has begun to look into the possibly evolutional origins of newly identified
543 transporters although, as yet, observations are preliminary and await further analysis
544 to clarify specific questions, as demonstrated in the detailed evolutionary analysis of
545 chloroplast transporters (Karkar et al., 2015). Our further analysis on the phenotypes
546 of two of these transporters, AMT1 and AMT2, using parasites depleted with these
547 activities, demonstrates differing degrees of defects at critical points in the parasite's
548 physiology and metabolism. We also observed similar decreases in level of the MEP
549 biosynthesis activity upon depletion of AMT1 and AMT2, indicating that phenotypic
550 outcomes did not result from apicoplast abnormality, since other phenotypic outcomes
551 were more severe in the AMT2-depleted parasites. We predict, therefore, that the
552 metabolic defects possibly result from a reduced supply of substrates by each of the
553 transporter. It is noteworthy that other studies provided us comparable knowledge in
554 phenotypes in TPC-depleted and APT1-depleted parasites. In these parasites,
555 metabolic defects in the apicoplast pathways were observed by indirect
556 measurements (Brooks et al., 2010; Li et al., 2021); however, these phenotypes were
557 possibly caused by pleitropic effects of apicoplast loss, since they were analyzed by a
558 comparably slow inactivation system to deplete the transporters of TPC and APT1

(with an induction of at least 3-4 days). Nevertheless, in our case with a highly efficient inactivation system, we still cannot exclude the effect of apicoplast loss on phenotypic results caused by depletion of the AMTs. Therefore, a more precise understanding of the functions of the AMTs will require further identification of the topology, protein interactions and substrate transport capability in the complex configuration of the apicoplast membranes. Our work, as yet, unsuccessful, in attempting to use a pyruvate sensor and/or a heterologous expression the AMTs in *E. coli*, is the first attempt to examine the transport capability of pyruvate by AMT1 and AMT2. Thereafter, application of more sophisticated approaches, such as *Xenopus* oocytes, an improved *E. coli* system, or a yeast expression system, may enable us to tackle the important question of substrate transport by AMT1 and AMT2. Future progresses on this direction will thus shed critical insights into the discrepancies in parasite growth that we observe when comparing cell culture versus infections in mice.

REFERENCES

Alaganan, A., Fentress, S.J., Tang, K., Wang, Q., and Sibley, L.D. (2014). *Toxoplasma* GRA7 effector increases turnover of immunity-related GTPases and contributes to acute virulence in the mouse. Proc Natl Acad Sci U S A *111*, 1126-1131.

Arce-Molina, R., Cortes-Molina, F., Sandoval, P.Y., Galaz, A., Alegria, K., Schirmeier, S., Barros, L.F., and San Martin, A. (2020). A highly responsive pyruvate sensor reveals pathway-regulatory role of the mitochondrial pyruvate carrier MPC. Elife *9*.

Barylyuk, K., Koreny, L., Ke, H., Butterworth, S., Crook, O.M., Lassadi, I., Gupta, V., Tromer, E., Mourier, T., Stevens, T.J.*, et al.* (2020). A Comprehensive Subcellular Atlas of the *Toxoplasma* Proteome via hyperLOPIT Provides Spatial Context for Protein Functions. Cell Host Microbe *28*, 752-766 e759.

Boucher, M.J., Ghosh, S., Zhang, L., Lal, A., Jang, S.W., Ju, A., Zhang, S., Wang, X., Ralph, S.A., Zou, J.*, et al.* (2018). Integrative proteomics and bioinformatic prediction enable a high-confidence apicoplast proteome in malaria parasites. PLoS Biol *16*, e2005895.

Branon, T.C., Bosch, J.A., Sanchez, A.D., Udeshi, N.D., Svinkina, T., Carr, S.A., Feldman, J.L., Perrimon, N., and Ting, A.Y. (2018). Efficient proximity labeling in living cells and organisms with TurboID. Nat Biotechnol *36*, 880-887.

Bricker, D.K., Taylor, E.B., Schell, J.C., Orsak, T., Boutron, A., Chen, Y.C., Cox, J.E., Cardon, C.M., Van Vranken, J.G., Dephoure, N.*, et al.* (2012). A mitochondrial pyruvate carrier required for pyruvate uptake in yeast, Drosophila, and humans. Science *337*, 96-100.

Brooks, C.F., Johnsen, H., van Dooren, G.G., Muthalagi, M., Lin, S.S., Bohne, W., Fischer, K., and Striepen, B. (2010). The *toxoplasma* apicoplast phosphate translocator links cytosolic and apicoplast metabolism and is essential for parasite survival. Cell Host Microbe *7*, 62-73.

Brown, K.M., Long, S., and Sibley, L.D. (2017). Plasma Membrane Association by N-Acylation Governs PKG Function in *Toxoplasma gondii*. mBio *8*.

Brown, K.M., Long, S., and Sibley, L.D. (2018). Conditional Knockdown of Proteins Using Auxin-inducible Degron (AID) Fusions in Toxoplasma gondii. Bio Protoc *8*.

Brown, K.M., and Sibley, L.D. (2018). Essential cGMP Signaling in *Toxoplasma* Is Initiated by a Hybrid P-Type ATPase-Guanylate Cyclase. Cell Host Microbe *24*, 804-816 e806.

Carruthers, V.B., Sherman, G.D., and Sibley, L.D. (2000). The *Toxoplasma* adhesive protein MIC2 is proteolytically processed at multiple sites by two parasite-derived proteases. J Biol Chem *275*, 14346-14353.

Cavalier-Smith, T. (1999). Principles of protein and lipid targeting in secondary symbiogenesis: euglenoid, dinoflagellate, and sporozoan plastid origins and the eukaryote family tree. J Eukaryot Microbiol *46*, 347-366.

Cavalier-Smith, T. (2000). Membrane heredity and early chloroplast evolution. Trends Plant Sci *5*, 174-182.

Daberkow, R.L., White, B.R., Cederberg, R.A., Griffin, J.B., and Zempleni, J. (2003). Monocarboxylate transporter 1 mediates biotin uptake in human peripheral blood mononuclear cells. J Nutr *133*, 2703-2706.

DeRocher, A.E., Coppens, I., Karnataki, A., Gilbert, L.A., Rome, M.E., Feagin, J.E., Bradley, P.J., and Parsons, M. (2008). A thioredoxin family protein of the apicoplast periphery identifies abundant candidate transport vesicles in *Toxoplasma gondii*. Eukaryot Cell *7*, 1518-1529.

Dou, Z., McGovern, O.L., Di Cristina, M., and Carruthers, V.B. (2014). *Toxoplasma gondii* ingests and digests host cytosolic proteins. mBio *5*, e01188-01114.

Fata, J.J., and Rabuzzi, D.D. (1988). Aggressive juvenile fibromatosis presenting as a parotid mass. Ear Nose Throat J *67*, 678, 681-672, 684 passim.

Felmlee, M.A., Jones, R.S., Rodriguez-Cruz, V., Follman, K.E., and Morris, M.E. (2020). Monocarboxylate Transporters (SLC16): Function, Regulation, and Role in Health and Disease. Pharmacol Rev *72*, 466-485.

Fleige, T., Fischer, K., Ferguson, D.J., Gross, U., and Bohne, W. (2007). Carbohydrate metabolism in the *Toxoplasma gondii* apicoplast: localization of three glycolytic isoenzymes, the single pyruvate dehydrogenase complex, and a plastid phosphate translocator. Eukaryot Cell *6*, 984-996.

Foth, B.J., Ralph, S.A., Tonkin, C.J., Struck, N.S., Fraunholz, M., Roos, D.S., Cowman, A.F., and McFadden, G.I. (2003). Dissecting apicoplast targeting in the malaria

parasite *Plasmodium falciparum*. Science *299*, 705-708.
Furumoto, T. (2016). Pyruvate transport systems in organelles: future directions in C4 biology research. Curr Opin Plant Biol *31*, 143-148.
Furumoto, T., Yamaguchi, T., Ohshima-Ichie, Y., Nakamura, M., Tsuchida-Iwata, Y., Shimamura, M., Ohnishi, J., Hata, S., Gowik, U., Westhoff, P.*, et al.* (2011). A plastidial sodium-dependent pyruvate transporter. Nature *476*, 472-475.
Gao, X., Pujos-Guillot, E., and Sebedio, J.L. (2010). Development of a quantitative metabolomic approach to study clinical human fecal water metabolome based on trimethylsilylation derivatization and GC/MS analysis. Anal Chem *82*, 6447-6456.
Gasperotti, A., Going, S., Fajardo-Ruiz, E., Forne, I., and Jung, K. (2020). Function and Regulation of the Pyruvate Transporter CstA in *Escherichia coli*. Int J Mol Sci *21*.
Gould, S.B., Waller, R.F., and McFadden, G.I. (2008). Plastid evolution. Annu Rev Plant Biol *59*, 491-517.
Gu, Z., Eils, R., and Schlesner, M. (2016). Complex heatmaps reveal patterns and correlations in multidimensional genomic data. Bioinformatics *32*, 2847-2849.
Harding, C.R., Sidik, S.M., Petrova, B., Gnadig, N.F., Okombo, J., Herneisen, A.L., Ward, K.E., Markus, B.M., Boydston, E.A., Fidock, D.A.*, et al.* (2020). Genetic screens reveal a central role for heme metabolism in artemisinin susceptibility. Nat Commun *11*, 4813.
Heaslip, A.T., Dzierszinski, F., Stein, B., and Hu, K. (2010). TgMORN1 is a key organizer for the basal complex of *Toxoplasma gondii*. PLoS Pathog *6*, e1000754.
Herzig, S., Raemy, E., Montessuit, S., Veuthey, J.L., Zamboni, N., Westermann, B., Kunji, E.R., and Martinou, J.C. (2012). Identification and functional expression of the mitochondrial pyruvate carrier. Science *337*, 93-96.
Howe, R., Kelly, M., Jimah, J., Hodge, D., and Odom, A.R. (2013). Isoprenoid biosynthesis inhibition disrupts Rab5 localization and food vacuolar integrity in *Plasmodium falciparum*. Eukaryot Cell *12*, 215-223.
Huynh, M.H., and Carruthers, V.B. (2009). Tagging of endogenous genes in a *Toxoplasma gondii* strain lacking Ku80. Eukaryot Cell *8*, 530-539.
Janouskovec, J., Horak, A., Obornik, M., Lukes, J., and Keeling, P.J. (2010). A common red algal origin of the apicomplexan, dinoflagellate, and heterokont plastids. Proc Natl Acad Sci U S A *107*, 10949-10954.
Karkar, S., Facchinelli, F., Price, D.C., Weber, A.P., and Bhattacharya, D. (2015). Metabolic connectivity as a driver of host and endosymbiont integration. Proc Natl Acad Sci U S A *112*, 10208-10215.
Karnataki, A., Derocher, A., Coppens, I., Nash, C., Feagin, J.E., and Parsons, M. (2007). Cell cycle-regulated vesicular trafficking of *Toxoplasma* APT1, a protein localized to multiple apicoplast membranes. Mol Microbiol *63*, 1653-1668.
Karnataki, A., DeRocher, A.E., Feagin, J.E., and Parsons, M. (2009). Sequential processing of the *Toxoplasma* apicoplast membrane protein FtsH1 in topologically distinct domains during intracellular trafficking. Mol Biochem Parasitol *166*, 126-133.
Kennedy, K., Cobbold, S.A., Hanssen, E., Birnbaum, J., Spillman, N.J., McHugh, E., Brown, H., Tilley, L., Spielmann, T., McConville, M.J.*, et al.* (2019a). Delayed death in

the malaria parasite *Plasmodium falciparum* is caused by disruption of prenylation-dependent intracellular trafficking. PLoS Biol *17*, e3000376.

Kennedy, K., Crisafulli, E.M., and Ralph, S.A. (2019b). Delayed Death by Plastid Inhibition in Apicomplexan Parasites. Trends Parasitol *35*, 747-759.

Kloehn, J., Lacour, C.E., and Soldati-Favre, D. (2021). The metabolic pathways and transporters of the plastid organelle in Apicomplexa. Curr Opin Microbiol *63*, 250-258.

Knappe, S., Flugge, U.I., and Fischer, K. (2003). Analysis of the plastidic phosphate translocator gene family in Arabidopsis and identification of new phosphate translocator-homologous transporters, classified by their putative substrate-binding site. Plant Physiol *131*, 1178-1190.

Krishnan, A., Kloehn, J., Lunghi, M., Chiappino-Pepe, A., Waldman, B.S., Nicolas, D., Varesio, E., Hehl, A., Lourido, S., Hatzimanikatis, V.*, et al.* (2020). Functional and Computational Genomics Reveal Unprecedented Flexibility in Stage-Specific *Toxoplasma* Metabolism. Cell Host Microbe *27*, 290-306 e211.

Li, Z.H., King, T.P., Ayong, L., Asady, B., Cai, X., Rahman, T., Vella, S.A., Coppens, I., Patel, S., and Moreno, S.N.J. (2021). A plastid two-pore channel essential for inter-organelle communication and growth of *Toxoplasma gondii*. Nat Commun *12*, 5802.

Li, Z.H., Ramakrishnan, S., Striepen, B., and Moreno, S.N. (2013). *Toxoplasma gondii* relies on both host and parasite isoprenoids and can be rendered sensitive to atorvastatin. PLoS Pathog *9*, e1003665.

Liang, X., Cui, J., Yang, X., Xia, N., Li, Y., Zhao, J., Gupta, N., and Shen, B. (2020). Acquisition of exogenous fatty acids renders apicoplast-based biosynthesis dispensable in tachyzoites of *Toxoplasma*. J Biol Chem *295*, 7743-7752.

Lim, L., Linka, M., Mullin, K.A., Weber, A.P., and McFadden, G.I. (2010). The carbon and energy sources of the non-photosynthetic plastid in the malaria parasite. FEBS Lett *584*, 549-554.

Lim, L., and McFadden, G.I. (2010). The evolution, metabolism and functions of the apicoplast. Philos Trans R Soc Lond B Biol Sci *365*, 749-763.

Long, S., Anthony, B., Drewry, L.L., and Sibley, L.D. (2017a). A conserved ankyrin repeat-containing protein regulates conoid stability, motility and cell invasion in *Toxoplasma gondii*. Nat Commun *8*, 2236.

Long, S., Brown, K.M., Drewry, L.L., Anthony, B., Phan, I.Q.H., and Sibley, L.D. (2017b). Calmodulin-like proteins localized to the conoid regulate motility and cell invasion by *Toxoplasma gondii*. PLoS Pathog *13*, e1006379.

Long, S., Brown, K.M., and Sibley, L.D. (2018). CRISPR-mediated Tagging with BirA Allows Proximity Labeling in *Toxoplasma gondii*. Bio Protoc *8*.

Long, S., Wang, Q., and Sibley, L.D. (2016). Analysis of Noncanonical Calcium-Dependent Protein Kinases in *Toxoplasma gondii* by Targeted Gene Deletion Using CRISPR/Cas9. Infect Immun *84*, 1262-1273.

Low, L.M., Stanisic, D.I., and Good, M.F. (2018). Exploiting the apicoplast: apicoplast-targeting drugs and malaria vaccine development. Microbes Infect *20*, 477-483.

McFadden, G.I., and Roos, D.S. (1999). Apicomplexan plastids as drug targets. Trends Microbiol *7*, 328-333.
McFadden, G.I., and Yeh, E. (2017). The apicoplast: now you see it, now you don't. Int J Parasitol *47*, 137-144.
Mullin, K.A., Lim, L., Ralph, S.A., Spurck, T.P., Handman, E., and McFadden, G.I. (2006). Membrane transporters in the relict plastid of malaria parasites. Proc Natl Acad Sci U S A *103*, 9572-9577.
Niu, Z., Ye, S., Liu, J., Lyu, M., Xue, L., Li, M., Lyu, C., Zhao, J., and Shen, B. (2022). Two apicoplast dwelling glycolytic enzymes provide key substrates for metabolic pathways in the apicoplast and are critical for *Toxoplasma* growth. PLoS Pathog *18*, e1011009.
Obornik, M., Janouskovec, J., Chrudimsky, T., and Lukes, J. (2009). Evolution of the apicoplast and its hosts: from heterotrophy to autotrophy and back again. Int J Parasitol *39*, 1-12.
Pao, S.S., Paulsen, I.T., and Saier, M.H., Jr. (1998). Major facilitator superfamily. Microbiol Mol Biol Rev *62*, 1-34.
Plattner, F., and Soldati-Favre, D. (2008). Hijacking of host cellular functions by the Apicomplexa. Annu Rev Microbiol *62*, 471-487.
Ralph, S.A., van Dooren, G.G., Waller, R.F., Crawford, M.J., Fraunholz, M.J., Foth, B.J., Tonkin, C.J., Roos, D.S., and McFadden, G.I. (2004). Tropical infectious diseases: metabolic maps and functions of the *Plasmodium falciparum* apicoplast. Nat Rev Microbiol *2*, 203-216.
Ramakrishnan, S., Docampo, M.D., Macrae, J.I., Pujol, F.M., Brooks, C.F., van Dooren, G.G., Hiltunen, J.K., Kastaniotis, A.J., McConville, M.J., and Striepen, B. (2012). Apicoplast and endoplasmic reticulum cooperate in fatty acid biosynthesis in apicomplexan parasite *Toxoplasma gondii*. J Biol Chem *287*, 4957-4971.
Salomaki, E.D., and Kolisko, M. (2019). There Is Treasure Everywhere: Reductive Plastid Evolution in Apicomplexa in Light of Their Close Relatives. Biomolecules *9*.
Sayers, C.P., Mollard, V., Buchanan, H.D., McFadden, G.I., and Goodman, C.D. (2018). A genetic screen in rodent malaria parasites identifies five new apicoplast putative membrane transporters, one of which is essential in human malaria parasites. Cell Microbiol *20*.
Sidik, S.M., Huet, D., Ganesan, S.M., Huynh, M.H., Wang, T., Nasamu, A.S., Thiru, P., Saeij, J.P.J., Carruthers, V.B., Niles, J.C.*, et al.* (2016). A Genome-wide CRISPR Screen in *Toxoplasma* Identifies Essential Apicomplexan Genes. Cell *166*, 1423-1435 e1412.
Sleda, M.A., Li, Z.H., Behera, R., Baierna, B., Li, C., Jumpathong, J., Malwal, S.R., Kawamukai, M., Oldfield, E., and Moreno, S.N.J. (2022). The Heptaprenyl Diphosphate Synthase (Coq1) Is the Target of a Lipophilic Bisphosphonate That Protects Mice against *Toxoplasma gondii* Infection. mBio *13*, e0196622.
Soldati, D., and Boothroyd, J.C. (1993). Transient transfection and expression in the obligate intracellular parasite *Toxoplasma gondii*. Science *260*, 349-352.
Striepen, B. (2011). The apicoplast: a red alga in human parasites. Essays Biochem

51, 111-125.
Swift, R.P., Rajaram, K., Keutcha, C., Liu, H.B., Kwan, B., Dziedzic, A., Jedlicka, A.E., and Prigge, S.T. (2020). The NTP generating activity of pyruvate kinase II is critical for apicoplast maintenance in *Plasmodium falciparum*. Elife *9*.
Tjhin, E.T., Hayward, J.A., McFadden, G.I., and van Dooren, G.G. (2020). Characterization of the apicoplast-localized enzyme TgUroD in *Toxoplasma gondii* reveals a key role of the apicoplast in heme biosynthesis. J Biol Chem *295*, 1539-1550.
Tyra, H.M., Linka, M., Weber, A.P., and Bhattacharya, D. (2007). Host origin of plastid solute transporters in the first photosynthetic eukaryotes. Genome Biol *8*, R212.
van Dooren, G.G., Tomova, C., Agrawal, S., Humbel, B.M., and Striepen, B. (2008). *Toxoplasma gondii* Tic20 is essential for apicoplast protein import. Proc Natl Acad Sci U S A *105*, 13574-13579.
Vaughan, A.M., O'Neill, M.T., Tarun, A.S., Camargo, N., Phuong, T.M., Aly, A.S., Cowman, A.F., and Kappe, S.H. (2009). Type II fatty acid synthesis is essential only for malaria parasite late liver stage development. Cell Microbiol *11*, 506-520.
Waller, R.F., Keeling, P.J., Donald, R.G., Striepen, B., Handman, E., Lang-Unnasch, N., Cowman, A.F., Besra, G.S., Roos, D.S., and McFadden, G.I. (1998). Nuclear-encoded proteins target to the plastid in *Toxoplasma gondii* and *Plasmodium falciparum*. Proc Natl Acad Sci U S A *95*, 12352-12357.
Walmsley, A.R., Barrett, M.P., Bringaud, F., and Gould, G.W. (1998). Sugar transporters from bacteria, parasites and mammals: structure-activity relationships. Trends Biochem Sci *23*, 476-481.
Wan, W., Dong, H., Lai, D.H., Yang, J., He, K., Tang, X., Liu, Q., Hide, G., Zhu, X.Q., Sibley, L.D.*, et al.* (2023). The *Toxoplasma* micropore mediates endocytosis for selective nutrient salvage from host cell compartments. Nat Commun *14*, 977.
Weber, A.P., Linka, M., and Bhattacharya, D. (2006). Single, ancient origin of a plastid metabolite translocator family in Plantae from an endomembrane-derived ancestor. Eukaryot Cell *5*, 609-612.
Xia, N., Ye, S., Liang, X., Chen, P., Zhou, Y., Fang, R., Zhao, J., Gupta, N., Yang, S., Yuan, J.*, et al.* (2019). Pyruvate Homeostasis as a Determinant of Parasite Growth and Metabolic Plasticity in *Toxoplasma gondii*. mBio *10*.
Yeh, E., and DeRisi, J.L. (2011). Chemical rescue of malaria parasites lacking an apicoplast defines organelle function in blood-stage *Plasmodium falciparum*. PLoS Biol *9*, e1001138.
Yesbolatova, A., Saito, Y., Kitamoto, N., Makino-Itou, H., Ajima, R., Nakano, R., Nakaoka, H., Fukui, K., Gamo, K., Tominari, Y.*, et al.* (2020). The auxin-inducible degron 2 technology provides sharp degradation control in yeast, mammalian cells, and mice. Nat Commun *11*, 5701.
Zhang, M., Wang, C., Otto, T.D., Oberstaller, J., Liao, X., Adapa, S.R., Udenze, K., Bronner, I.F., Casandra, D., Mayho, M.*, et al.* (2018). Uncovering the essential genes of the human malaria parasite *Plasmodium falciparum* by saturation mutagenesis. Science *360*.

Zuther, E., Johnson, J.J., Haselkorn, R., McLeod, R., and Gornicki, P. (1999). Growth of *Toxoplasma gondii* is inhibited by aryloxyphenoxypropionate herbicides targeting acetyl-CoA carboxylase. Proc Natl Acad Sci U S A *96*, 13387-13392.

ACKNOWLEDGMENTS

We are grateful to Dr. Sophie Alvarez and Dr. Michael Naldrett at the Proteomics and Metabolomics Facility, Center for Biotechnology at the University of Nebraska-Lincoln for the proteomics analysis, Dr. Wen-Chao Wang at the Shanghai Profleader Biotech Co., Ltd for untargeted metabolomics analysis, and the imaging center at the School of Life Sciences, Sun Yat-Sun University for assistance with TEM and immuno-EM. We thank Prof. Vern Carruthers for the kind gift of RH*Δku80Δhxgprt* line, and Prof. Philippe Bastin for monoclonal antibodies against the epitope tag Ty (BB2).

This research was supported by the National Key Research and Development Program of China (Grant Nos. 2021YFC2300800 and 2021YFC2300802) to X.Q. Z, by the National Natural Science Foundation of China (31873009 to S.L. and 31772445 to D.H.L), and by the University Startup Package to S.L..

Author Contributions

Conceptualization, S.L.; Methodology, H.D.; J.Y.; K.H.; W.B.Z.; J.L.; Investigation, H.D.; J.Y.; K.H.; W.B.Z.; H.Y.D.; R.B.W.; Formal Analysis, S.L.; H.D.; K.H.; J.Y.; D.H.L. Writing – Original Draft, S.L.; Writing – Review & Editing, S.L.; G.H.; K.M.B.; X.Q.Z.; D.H.L.;Z.R.L.; Funding Acquisition, X.Q.Z.; S.L.; D.H.L.; Resources, S.L.; D.H.L.; X.Q.Z.; Supervision, S.L..

DECLARATION OF INTERESTS

The authors declare no competing interests.

836 **Materials and Methods**

837 **Reagents and Antibodies**

838 All chemicals were obtained from Sigma or ThermoFisher Scientific unless otherwise
839 stated. Secondary antibodies used for immunofluorescence were conjugated to Alexa
840 Fluor 488, Alexa Fluor 568, or Alexa Fluor 350 and were purchased from Invitrogen.
841 Secondary antibodies used for western blots were IRDye 800CW or 680CW
842 conjugates and were purchased from from LI-COR. Primary antibodies were listed as
843 follows: rabbit anti-HA (Thermofisher, #71-5500), mouse anti-HA (BioLegend,
844 #901501), mouse anti-C-myc (BioLegend, #626801), mouse anti-GFP (Thermofisher,
845 #MA5-15349), mouse mAb 6D10 anti-MIC2 (Carruthers et al., 2000), rabbit
846 anti-GRA7 (Alaganan et al., 2014) and mouse anti-Ty (BB2) antibodies. Antibodies,
847 such as rabbit anti-ACP, rabbit anti-actin, mouse anti-IMC1, and rabbit anti-GAP45,
848 were generated in our recent study (Wan et al., 2023).

849 **Parasite and cell culture**

850 *T. gondii* RHΔ*hxgprt*Δ*ku80* (Huynh and Carruthers, 2009), RHΔ*hxgprt*Δ*ku80*/TIR1
851 (Brown et al., 2017) and their derivative lines were listed in Table S2. The tachyzoite
852 lines were grown in human foreskin fibroblast (HFF-1 from ATCC SCRC-1041) in D5
853 media prepared by DMEM supplemented with 5% inactivated fetal bovine serum (FBS)
854 (Transgene, FS201-02), 10 mM glutamine and penicillin-streptomycin. The lines and
855 HFF-1 were maintained mycoplasma negative as described previously (Long et al.,
856 2016). The TIR1 and AID lines were cultured in HFF-1 with 500 μM auxin (+IAA) or
857 0.1% ethanol alone (-IAA) for phenotypic assays, as previously described (Brown et
858 al., 2017; Long et al., 2017b). Parasites were harvested by passing through 22g
859 needles and by filtration through 3.0 micron polycarbonate membranes, from which
860 extracellular parasites were used for experimental assays.

861 **Mice**

862 *T. gondii* parasite growth *in vivo* was tested in six-week old BALB/C mice. Mice were
863 maintained under specific pathogen-free (SPF) conditions in filter-top cages with
864 provision of sterile water and food. Mice were randomly assigned to experimental
865 groups (n=5 per group), and challenged by intraperitoneal (i.p.) injection of 100 *T.*
866 *gondii* tachiyzoites, following by monitoring on a daily basis to record their health by
867 checking their appearance, bodyweight and responsiveness. The mouse experiments
868 were conducted according to the guidelines and regulations issued by the Veterinary
869 Office of the China Agricultural University (Issue No. AW11402202-2-1).

870 **Generation of Plasmids and *T. gondii* Lines**

871 A CRISPR/Cas9 sgRNA 3' plasmid (Table S3) targeting a region close to a stop codon
872 at a specific gene can efficiently produce Cas9 and sgRNA to create DNA double
873 strand breaks (DSB) in parasites, which facilitates the integration of a tagging
874 amplicon at the 3' terminus of a specific gene. The sgRNA specific sequences were
875 selected, as described in our previous protocol (Brown et al., 2018). The sequences
876 were integrated into the pCas9 plasmid using a basic seamless cloning and assembly
877 kit (CU201-02, TransGen Biotech) with primers listed in Table S4, as described in our
878 recent study (manuscript in press). The amplicon for a specific integration at the DSB
879 was generated from a generic tagging plasmid (Table S3) using a pair of primers L
880 and T (Table S4), as described in our previous study (Long et al., 2017b), which was
881 illustrated in Fig. S$A. These generic plasmids included pL-6Ty-HXGPRT (Brown and
882 Sibley, 2018), pL-6HA-DHFR (Long et al., 2017a), pL-6HA-HXGPRT (addgene
883 #86552) (Long et al., 2017b), pL-TurboID-4Ty-DHFR (manuscript in press),
884 pL-AID-6Ty-DHFR (manuscript in press) and pL-AID-3HA-HXGPRT (addgene #86553)
885 (Long et al., 2017b). One additional generic plasmid pL-AID-GFP-HXGPRT was
886 generated using pL-AID-3HA-HXGPRT as the PCR template of plasmid backbone,
887 followed by cloning the GFP fragment into the backbone with primers listed in Table
888 S4. The amplicon generated by primers L and T from the generic plasmids contains
889 short homologs (HR1 and HR2, 41 bp) for targeting the upstream (HR1) of the stop

890 codon and the downstream (HR2) of the Cas9 cleavage site (DSB), resulting in
891 integration of epitope tags or AID fragments in frame with the encoding sequences of
892 specific genes. The drug-selected lines were sub-cloned, followed with screening with
893 diagnostic PCR, IFA and western blots. The resistance markers containing LoxP sites
894 can be excised by transfection with pmini-Cre, as previously described (Heaslip et al.,
895 2010).

896 **Transfection and Selection**

897 Parasites were harvested and resuspended in Cytomix (10 mM KPO_4, 120 mM KCl, 5
898 mM $MgCl_2$, 25 mM HEPES, 2 mM EDTA) $1x10^8$ parasites/ml, then combined with
899 10-20 µg pCas9-sgRNA 3' and 1-5 µg amplicons with 2 mM ATP, 2 mM GSH and 150
900 µM $CaCl_2$ to a final volume of 250 µl, followed with electroporation using a BTX ECM
901 830 electroporator (Harvard Apparatus), as described previously (Soldati and
902 Boothroyd, 1993). Parasites were selected on the second day with addition of
903 appropriate drugs mycophenolic acid (MPA) (25 µg/ml) and 6-xanthine (6Xa) (50
904 µg/ml), or pyrimethamine (Pyr) (3 µM). Negative selection was applied with
905 6-thio-xanthine (200 µg/ml) when parasites were transfected with a pCre plasmid to
906 remove the resistant marker HXGPRT. Positive selection pools of parasites were
907 subcloned in 96-well plates at 3 parasites/well, and allowed to grow for 6-7 days
908 before selection of wells containing a single plaque. Pure clones were diagnosed by
909 PCR using appropriate primers (Table S4) and IFA analysis using appropriate
910 antibodies if applicable.

911 **Indirect Fluorescence Assay (IFA)**

912 Parasites were fixed by 4% paraformaldehyde in PBS, followed by blocking and
913 permeabilization using PBS containing 2.5% BSA and 0.25% Triton X100. Antibody
914 incubation was performed with indicated combinations of primary antibodies for 30
915 min, followed by incubation with secondary antibodies conjugated with fluorescent
916 dyes (Thermofisher Scientific) for 30 min. The above procedures were applied to the

917 ACP diffusion analysis for parasites as stated in the results and legends. The blind
918 counting was conducted for at least 150 vacuoles (intracellular parasites) or single
919 parasites (extracellular parasites) in each replicate. ProLong Gold Antifade Mountant
920 with or without DAPI were used to mount the coverslips on glass slides. Parasites
921 were then imaged using a Nikon Ni-E microscope C2+ equipped with a DS-Ri2
922 Microscope Camera. The co-localization analyses were performed using the Ni-E
923 software system NIS Elements AR. All the IFA analyses were carefully repeated at
924 least three times, and similar results were obtained for the same experiments before
925 finalizing the analysis.

926 **Western blotting**

927 Parasites were resuspended in PBS, followed by addition of 5x Laemmli sample
928 buffer supplemented with 1 mM DTT for a further incubation at 98 °C for 10 min.
929 Protein lysis was then resolved in SDS-PAGE, blotted by a BioRad wet-blotting
930 system, subsequently incubated with different combinations of primary and secondary
931 antibodies, followed by secondary antibodies conjugated with LI-COR reagents, or
932 streptavidin LI-COR 800CW.. The blot membranes were then visualized by a Bio-RAD
933 ChemiDOC MP system.

934 **TurboID and Biotinylated Proteins**

935 The APT1-TurboID line was grown on HFF monolayers for 24 hours, subsequently
936 incubated with 500 μM D-biotin for 90 min. The parasites were fixed with 4%
937 paraformaldehyde solution for IFA or harvested for western blots. IFA and western
938 blots were performed with appropriate streptavidin reagents to visualize biotinylated
939 proteins in parasites. The parental line and APT1-TurboID line were grown in HFF
940 cells for 36 hours, followed with labeling of proteins by 500 μM D-biotin for 90 min, and
941 harvesting of the parasites for purification of biotinylated proteins. In parallel, the
942 APT1-TurboID parasites after 36 hours growing were harvested, and extracellular
943 parasites were incubated with 500 μM D-biotin for 90 min, followed with by collection

944 of parasites for purification of biotinylated proteins. The parasites were lysed in a
945 buffer containing 1% Triton X-100, 0.2% SDS and 0.5% deoxycholate, and sonicated
946 with a microtip in 550 sonic dismembrator (ThermoFisher Scientific). Biotinylated
947 proteins in cleared supernatant were purified using streptavidin magnetic beads,
948 exactly following the protocol described elsewhere (Long et al., 2018).

949 **Proteomic analysis**

950 The purified proteins were separated on SDS-PAGE and stained by Coomassie blue
951 R250, 45% methanol and 10% glacial acetic acid, subsequently dried on SDS-PAGE
952 slices by vacuum. The dried gels were rehydrated, alkylated and washed to remove
953 the stain and SDS, and subjected to steps of mass-spectrometry analysis, following
954 the protocol described in the Bio-Protocol (Long et al., 2018). The parental line and
955 TurboID fusion line were analyzed in parallel with three technical and biological
956 replicates. Resulting spectra were searched against a combined database of *T. gondii*
957 ME49 (http://ToxoDB.org, release 29) and human proteins and a decoy database,
958 using Mascot and Scaffold. The current views in Scaffold were exported into an excel
959 spreadsheet using the following settings of peptide 2, protein threshold 99% and
960 peptide threshold 95%. Hits were analyzed using embedded tools in ToxoDB
961 (https://toxodb.org/toxo/app/) to predict the transmembrane domain. Peptide numbers
962 of the hits in the TurboID were compared to those in the parental line (0 peptide was
963 considered as 1), and fold changes were used to plot a volcano map against $Log10^{p}$
964 ^{value} in ggplot2 package in R.

965 **Conservation and phylogenetic analysis**

966 The apicoplast proteins identified in this study and known apicoplast proteins as listed
967 in the results (Table S10) were used as queries for searching orthologues in
968 organisms in Eukaryote, including species belonging to the chromalveolates, plants,
969 metazoan and fungi, and Bacteria (Table S9). These proteins were simultaneously
970 searched with the profile Hidden Markov models (HMMs) search engine

971 (jackhammer). The E-value cutoff was set at 1e-7 and hits with an E-value < 1e-7
972 were considered as orthologues. The best hits from the representative species in
973 above taxa were merged and resultant list of orthologues (Table S10) were used for
974 conservation analysis with ComplexHeatmap package in R (v4.2.0) (Gu et al., 2016).
975 This analysis pulled up the protein conservation heatmap, with indication by a heat
976 scaled with E-value for each individual orthologue. The tree dendrogram without
977 meaningful branch lengths across these species, and across the proteins were
978 clustered according to the Euclidean distance using UPGMA method.
979 Representatives from the known apicoplast proteins were analyzed in parallel as the
980 control for comparison.

981 **Plaque Formation**

982 Parasites (150 parasites) were inoculated on confluent HFF monolayers in one 6-well
983 in plates, followed with addition of either 500 μM IAA or ethanol alone (0.1%) and
984 growth in D5 media at 37°C for 7 days. The parasites and monolayers were then fixed
985 with 70% ethanol for 15 min, stained with 0.5% crystal violet for 5 min, subsequently
986 washed with dH2O and dried at room temperature. The plaque monolayers were
987 recorded by scanning using a HP Scanjet G4050, and plaque numbers and plaque
988 sizes were measured in ImageJ.

989 **Parasite Replication**

990 The TIR1 and its derived AID lines were grown in 500 μM IAA for 24 hours on
991 monolayers in 24-well plates with coverslips. The parasites were fixed with 4%
992 paraformaldehyde for 10 min, followed with blocking and permeabilization with 0.25%
993 Triton X-100 in PBS containing 2.5% BSA. The parasites were then incubated with
994 GAP45 antibodies and secondary anti-rabbit antibodies conjugated with Alexa Fluor
995 568. The coverslips were mounted and visualized under a Nikon Ni-E microscope C+.
996 Vacuoles containing different numbers of parasites were scored on the same images
997 with blindness, and at least 150 vacuoles were counted in each replicate of three

998 independent experiments. Ratios of vacuoles containing different numbers of
999 parasites were plotted against the total vacuoles examined.

1000 **GFP acquisition assay**

1001 HFF cells expressing cytosolic GFP were prepared in our previous study (manuscript
1002 in press). In brief, pLVX-EF1a-GFP-IRES-puromycin was combined with packaging
1003 plasmids psPAX2 (addgene #12260) and pMD2.G (addgene #12259) in Opti-MEM I
1004 (31985062, Gibco), and mixed with Fugene HD (E2311, Promega), and transfected
1005 into 293T cells. Viruses were collected and mixed with polybrene in a 12-well plate
1006 well containing 30-50% confluent HFF-1 cell monolayers. After 24 hours of
1007 post-transduction, the cell monolayers were re-seeded with incubation of puromycin
1008 (2.5 μg/ml) for 3 days. The cell monolayers were then maintained and expanded in D5
1009 media. The TIR1 and AID lines were grown in the cell monolayers with IAA, 10 μM
1010 LHVS and 12.5 μM atorvastatin for 12, 24 or 36 hours. LHVS inhibits cysteine
1011 protease CPL to accumulate GFP derived from host cell cytosol, as reported
1012 previously (Dou et al., 2014), Atorvastatin can inhibit synthesis of FPP and GGPP in
1013 host cells, to decrease the supply of FPP and GGPP from the host cells to the
1014 parasites. In parallel, TIR1 was grown in the host cells with 10 μM LHVS, 0.3 μM
1015 zoledronic acid and 12.5 μM atorvastatin, serving as a positive control to observe
1016 defects in GFP transport by decreasing protein prenylation in parasites. The addition
1017 of atorvastatin and zoledronic acid could specifically inhibit the FPP and GGPP supply
1018 both in host cells and parasites (Li et al., 2013), thus inhibiting GFP transport to the
1019 VAC in parasites, as demonstrated in Fig. 5A-B. Purified parasites were adhered onto
1020 poly-lysine-coated coverslips, followed with fixation with 4% paraformaldehyde for 10
1021 min. The parasites were permeabilized by 0.25% Triton X-100 in PBS, subsequently
1022 mounted in ProLong Gold Antifade Mountant with DAPI for visualization under a Nikon
1023 Ni-E microscope C+. Parasites were judged by observations of parasites with either
1024 GFP foci, GFP diffusion or GFP absence, as demonstrated in Figure 4B.
1025 Fields/images were selected blind, and all parasites in the same images were counted

1026 for scoring of parasites with or without GFP signal. The counting was performed in
1027 replicate for at least 150 parasites. Percentages of parasites containing GFP foci were
1028 calculated and expressed as percentages in the populations.

1029 **Immuno-staining for Electron Microscopy (Immuno-EM)**

1030 Parasites were grown on HFF monolayers for 24 hours, subsequently digested with
1031 trypsin for collecting samples. Samples were fixed in a 0.1 M sodium cacodylate
1032 buffer (pH7.4) containing 3% (w/v) paraformaldehyde, 0.1% glutaraldehyde (v/v), 4%
1033 sucrose (w/v) at 4°C overnight. The samples were then washed four times by a 0.1 M
1034 sodium cacodylate buffer containing 4% (w/v) sucrose, and neutralized on ice by a 0.1
1035 M sodium cacodylate buffer containing 4% (w/v) sucrose, 0.1 M glycine, and
1036 dehydrated in ethanol. The samples were immersed in LR White resin (Ted Pella, Inc.)
1037 at 4°C overnight, subsequently polymerised at light intensity $1.2x10^5$ μJ/cm^2 on ice for
1038 5 hours. The LR White imbedded samples were sectioned with a Leica
1039 ultramicrotome (EM UC7) at 100 nm and were picked onto 100-mesh
1040 formvar-carbon-coated nickel grids. The loaded nickel grids were then blocked and
1041 incubated with mouse anti-Ty antibodies (1:5) at RT for 2 hours and overnight at 4°C,
1042 followed with washing by PBS. The samples on grids were incubated with Alexa
1043 FluorTM 488 goat anti-mouse IgG 10 nm colloidal gold particle (1:100) (15nm or 10
1044 nm in size) for 1 hours, followed with washs in PBS and double-distilled water. The
1045 samples on grids were stained by 3% phosphotungstic acid and observed under a
1046 JEM1400FLASH transmission electron microscope operation at 120 KV.

1047 **Transmission Electron Microscopy (TEM)**

1048 Parasites grown on HFF cell monolayers were collected by scraping off, fixed by a
1049 fixative mixture of 2% paraformaldehyde and 3% glutaraldehyde at 4 °C overnight.
1050 The samples were washed, fixed in 1% osmium tetroxide in 50 mM phosphate buffer
1051 at 4 °C for 1 hour, washed three times and dehydrated by sequential concentration of
1052 ethanol, and by acetone and Spurr for 1 hour. The samples were then imbedded in

1053 Spurr and sectioned to 100 nm slices by a Leica ultrmicrotome (EM UC7). The
1054 ultrathin-sections were collected on 100 mesh grids. The grids were then viewed by
1055 JEOL transmission electron microscopy (JEM1400FLASH).

1056 **Untargeted Metabolomics**

1057 Parasites were grown in IAA for 18 hours and purified in chilled PBS, followed by
1058 immediate quenching by addition of -40°C methanol and sterile ddH2O (400 µl
1059 methanol + 100 µl H_2O). The samples were processed for the analysis of metabolites
1060 by GC-MS and LC-MS, exactly following the protocol reported in our recent study
1061 (manuscript in press). Briefly, the GC-MS analysis was performed with An OPTIMA 5
1062 MS Accent fused-silica capillary column on Agilent7890A/5975C GC-MS system
1063 (Agilent Technologies Inc., CA, USA), while the LC-MS analysis was performed on a
1064 ThermoFisher Ultimate 3000 UHPLC system with a Waters ACQUITY UPLC BEH
1065 C18 column (2.1mm × 100 mm, 1.7µm) using standard positive and negative modes.
1066 For GC-MS, the peak picking, alignment, deconvolution and further processing of
1067 resulting raw data were carried out according to the previously published protocols
1068 (Gao et al., 2010). The final data was exported as a peak table file, including
1069 observations, variables (rt_mz), and peak areas. The data was normalized against the
1070 total peak value of total peaks, and differential metabolites were identified by
1071 statistical analysis performed in R platform, where parametric and nonparametric
1072 tests were done using One-way ANOVA with Dunnett's multiple comparison, to
1073 identify differential metabolites with $p<0.05$ and fold change >1.2 for further analysis.
1074 For LC-MS, The raw data was transformed to mzXML format by ProteoWizard and
1075 then processed by XCMS and CAMERA packages in R software platform. The final
1076 data was exported as a peak table file, including sample names, variables (rt_mz) and
1077 peak areas. The peak areas data was normalized to internal standards before the
1078 analysis of statistics. The in-house database was referenced to identify the compound
1079 by using m/z (MS1), mass spectra (MS2) and retention times (RT). Normalization for
1080 relative parasite amounts was based on the total integrated peak area values of

1081 metabolites within an experimental batch. Metabolites identified by the GCMS and
1082 LCMS were merged together for further analysis (Dataset S2). Enrichment of
1083 Metabolic Pathways (Table S13) were analyzed using the differential metabolites
1084 identified in three of the AID lines versus the TIR1 line. MetaboAnalyst 5.0 server was
1085 used to enrich the metabolite sets with KEGG, in which the *p*-value below 0.05 was
1086 considered to be significant.

1087 **Parasite growth in mice**

1088 Mice were randomly assigned to groups and were intraperitoneally injected with 100
1089 parasites per mouse. Subsequently, mice (n=5 mice for each line) were orally
1090 administered with IAA (3-indoleacetic acid, auxin, Sigma) and by an intraperitoneal
1091 injection on a daily basis (Brown and Sibley, 2018; Yesbolatova et al., 2020). The
1092 drinking water contained sterile water with 1 mg/ml IAA, 3 mM NaOH, 5% sucrose
1093 (w/v), flavored with 2 mg/ml TANG (Mondelēz International), pH8.0. Meanwhile, mice
1094 were intraperitoneally injected with a daily 0.2 ml of sterile solution containing 15
1095 mg/ml IAA, 1 M NaOH, pH7.8. The mice infected with the TIR1 line served as the
1096 control, which received the drinking water and injection of IAA-containing solution in
1097 the same way to the AID lines. The mice were weighted and their health conditions
1098 were monitored on a daily basis until day 20.

1099 **Quantification and statistical analysis**

1100 Experiments were conducted blind for at least two-three biological replicates and
1101 statistical analyses were conducted in Graphpad v8.0. One-way or two-way ANOVA
1102 with Tukey's multiple comparison was conducted for data that fit normal a distribution
1103 or the Mann-Whitney test for non-parametric comparison, while one-way ANOVA with
1104 Dunnett's multiple comparison was tested for data with small sizes or abnormal
1105 distributions. $p<0.05$ was considered significant. Experiment-specific statistical
1106 information is provided in the figure legends or associated method details including
1107 replicates (n), trials (N), and statistical tests performed.

1108 **Data availability**

1109 The proteomic data reported in this paper have been deposited in the OMIX, China
1110 National Center for Bioinformation/Beijing Institute of Genomics, Chinese Academy of
1111 Sciences (https://ngdc.cncb.ac.cn/omix) with accession number: WgSMCBqN. The
1112 metabolomics raw data have been deposited in the MetaboLights
1113 (https://www.ebi.ac.uk/metabolights/) with accession number: MTBLS7060. Minimally
1114 processed data of the proteomics and metabolomics data are available in Dataset S1
1115 and Dataset S2, respectively. *Toxoplasma gondii* genome information can be found in
1116 ToxoDB release 53 (http://toxodb.org) and Eukaryotic pathogen, Vector & Host
1117 Information Resources can be found in VEupathDB (http://veupathdb.org).

1118

1119

1120 **Figure Legends**

1121

1122 **Figure 1.** Discovery of apicoplast membrane proteins
1123 (A-B) Activity test of biotinylation of proximal proteins by APT1-TurboID-4Ty. Parasites
1124 were grown in 500 μM D-biotin for 90 min, followed by detection of biotinylated
1125 proteins (green) by streptavidin reagents on IFA (A), and on Western blots (B). Actin
1126 served as the loading control. Scale = 5 μm.
1127 (C) Volcano plot analysis comparing the TurboID fusion to the parental line. Three
1128 replicate mass-spectrometry experiments were analyzed by the student t-test. Known
1129 apicoplast proteins (red) and candidates with different numbers of TMDs (deep and
1130 light blue were indicated, and novel apicoplast proteins were pointed out. See Dataset
1131 S1.
1132 (D) Workflow of the discovery of novel apicoplast membrane proteins. Candidates
1133 from hyperLOPIT (Barylyuk et al., 2020), ACP-BirA (Boucher et al., 2018) and
1134 APT1-TurboID (this study) were screened by epitopte tagging and IFA.
1135 (E) Confocal co-localization of HAP-6Ty with the apicoplast marker ACP, showing

confocal imaging of HAP-6Ty (red) and ACP (green), and Pearson Corelation Coefficiency (PCC). The PCC values over the merged fluoresent foci for candidate proteins and ACP were analyzed by a co-localization and ROI intensity analysis module in the NIS Elements AR software and shown with mean ± SEM (N=6 for each). Scale = 5 μm.

(F-H) Summary and comparison of the screening from three datasets. The putative transporters are grouped into diverse types (F) and identified from three different datasets (G), which shared three novel proteins, as shown by the venn diagram (H). Three independent experiments were performed with similar outcomes (A, B, E).

Figure 2. Conservation analysis of putative transporters

(A-B) Heatmap indicating conservation of known apicoplast proteins and newly identified proteins among chromalveolates (A), red alga, green alga, plants, fungi, metazoa and bacteria (B). The conservation was scaled by a heat bar (red) with E-values for putative orthologues of the listed proteins (see Dataset S2). ToxoDB protein numbers (left) and protein (temporary) names (right) are shown. Their sequences were searched for orthologues using the Hidden Markov Model (HMM) (E value<E-7) and the best orthologue was used for the heatmap analysis in ComplexHeatmap package in R. Parasite fitness scores were shown on the right with the green heat bar for *T. gondii* (ToxoDB)(Sidik et al., 2016) and the blue bar for *P. falciparum* (PlasmoDB)(Zhang et al., 2018). The tree dendrogram across the genes were clustered according to the euclidean distance using UPGMA method. The species tree (top) shows phylogenetic relationships and major clades: *Theil*., *Theileria*; *Babes*, *Babesia*; *Crypt*., *Cryptosporidium*; *Proteo*, *Proteobacteria*.

Figure 3. AMT1 and AMT2 are localized at the apicoplast membrane and essential for parasite growth *in vitro*

(A) Western blot detection of protein depletion in the AID lines. The lines were induced

1164 by auxin (IAA) for different hours (hrs) as indicated. Western blots detected immatured
1165 (p) and matured (m) forms of the protein fusions in the non-induced lanes. Actin
1166 served as the control.
1167 (B) IFA detection of protein depletion in the AID lines. Parasites were grown in IAA for
1168 24 hours, followed by IFA with antibodies against Ty or HA (red) and IMC1 (green).
1169 Scale = 5 μm.
1170 (C-E) Plaque formation by the TIR1 and AID lines on HFF monolayers in ± IAA for 7
1171 days. Numbers (D) and sizes (E) of the plaques were measured by ImageJ. Scale =
1172 0.5 cm. Two independent experiments with triplicates were performed. Data are
1173 shown as a mean ± SEM.
1174 (F) Parasite replication of the TIR1 and AID lines grown in IAA. The parasites were
1175 grown in IAA for 24 hours, followed by scraping, harvesting and infection for the 2nd
1176 and 3rd rounds of parasite growth in IAA. The parasites stained with GFP45 were
1177 counted in vacuoles (at least 150 vacuoles in each replicate). In comparing to TIR1
1178 (1st, 2nd and 3rd), $p<0.0001$ for the AID lines with 2 and 8 parasites/vacuole in the 1st
1179 round, and for the AID lines with 1-8 parasites/vacuole in the 2nd round, $p<0.0001$ for
1180 the AID lines with 1 and 4 parasites/vacuoles in the 3rd round.
1181 (G-H) ACP diffusion in the TIR1 and AID lines grown in IAA. Parasites were grown in
1182 IAA for the 1st, 2nd and 3rd lytic cycles, as described in the parasite replication assay
1183 (intracellular parasites). Those parasites in the 1st and 2nd round of growth were forced
1184 to egress for the same analysis (extracellular parasites). Vacuoles or single parasites
1185 were scored (n>150 for each replicate).
1186 Fields/images were selected blind and all parasites/vacuoles were scored on the
1187 same fields/images (F-H). Three independent experiments were performed (A, B, F, G
1188 and H), data are shown as a mean ± SEM with two-way ANOVA with Tukey's multiple
1189 comparisons (compared with the TIR1). ***, $p<0.0001$.
1190
1191 **Figure 4.** Depletion of AMT1 and AMT2 caused defects of MEP and FASII pathways

1192 (A-C) The MEP activity was strongly affected in the AID lines. GFP transport to the
1193 VAC was assayed by growning parasties in GFP expressing HFF cells (HFF-GFP).
1194 LHVS (10 μM) was added to inhibit GFP digestion in the VAC (Dou et al., 2014). The
1195 isoprenoid synthesis in host cells and parasites was inhibited by IC50 concentrations
1196 of atorvastatin (10 μM) and zoledronate (0.3 μM)(Li et al., 2013), respectively (A). The
1197 inhibition over the TIR1 line using two of the drugs was used as a positive control (B).
1198 The AID parasites were grown in HFF-GFP cells in the presence of LHVS for 36 hours
1199 in total, with the addition of atorvastatin, zoledronate or IAA as stated for different
1200 experiments in the figure in the last 12 hours. Parasites were immediately harvested,
1201 adhered and scored, as shown in the example images in B. Percentages of parasites
1202 with GFP foci were plotted (C). Fields/images were selected blind and all
1203 parasites/vacuoles were scored on the same fields/images (C). Three independent
1204 experiments with triplicates were performed. Data are shown as a mean ± SEM with
1205 one-way ANOVA with Tukey's multiple comparison. ***, $p<0.0001$, scale = 5 μm.
1206 (D-F) Fatty acid synthesis and TCA metabolites were significantly reduced in IAA
1207 induced AID parasites. Parasites were grown in IAA for 18 hours and harvested for
1208 untargeted metabolomics with GCMS and LCMS (N=3), and metabolites detected
1209 were analyzed by Dunnette's multiple comparison by comparing the AID parasites to
1210 the TIR1. Three AID lines shared 13 differential metabolites (D). These shared
1211 metabolites included fatty acids and lipids, such as myristic acid, palmitoleic acid,
1212 oleic acid, and phosphatidylcholine (PC) (E), and metabolites related to the TCA cycle
1213 (F). *, $p<0.05$; **, $p<0.001$; ***, $p<0.0001$.
1214
1215 **Figure 5.** Examination of the apicoplast ultra-structures, and mouse virulence of the
1216 parasites upon depletion of the AID fusions.
1217 (A) Transmission electron microscopy (TEM) observed less electron dense or electron
1218 lucent lumen and loosened membranes in the apicoplast in the AID parasites induced
1219 in IAA for 24 hours. Representative images were shown. Scale = 200 nm.

1220 (B) Quantification of the apicoplast with the lumen less dense or lucent in parasites
1221 induced for 12, 24 and 36 hours and TIR in IAA for 36 hours. The TEM examined 300
1222 parasites for three lines (TIR1, AMT1-AID and AMT2-AID) at each time point, and
1223 numbers of abnormal apicoplast (red numbers) and apicoplast identified (green
1224 numbers) were shown by the columns. The columns express the percentages of
1225 abnormal apicoplast in all the identified apicoplasts.
1226 (C) Survival curve of BALB/C mice infected with 100 parasites intraperitoneally and
1227 treated with IAA for 20 days. The Gehan-Breslow-Wilcoxon test was used to compare
1228 differences between the survival curves (the AID line versus TIR1), ***, $p<0.0001$. The
1229 experiment of mouse infection was performed with 5 mice in each group, and results
1230 from three independent experiments (1st, 2nd and 3rd) were shown together with
1231 symbols for the mouse groups.
1232
1233
1234
1235 **Legends for Dataset S1-S2 and Table S5-12**
1236
1237 **Dataset S1.** Minimally processed mass spectrometry datasets of the APT1-TurboID
1238 fusion line and the parental line.
1239
1240 **Dataset S2**. Minimally processed datasets of untargeted metabolites detected by
1241 GCMS and LCMS in TIR1, AMT1-AID, AMT2-AID and dKD lines grown in IAA for 18
1242 hours.
1243
1244 **Table S5**. Volcano analysis of mass-spectrometry datasets from APT1-TurboID and
1245 the parental line. Intracellular and extracellular parasites of APT1-TurboID were
1246 incubated with 500 μM biotin for 1 hours, and biotinylated proteins were purified for
1247 Mass spectrometry analysis together with the control line RH. Datasets were analyzed

1248 by student t test and plotted by Volcano analysis.

1249 **Table S6**. List of known apicoplast proteins on the volcano plotting. The known
1250 proteins were listed with referenced PMID.

1251 **Table S7**. List of TMD proteins identified by APT1-TurboID and ordered from high
1252 numbers to low numbers. The MS hits identified from APT1-TurboID were analyzed in
1253 ToxoDB for identification of transmembrane domains (TMD).

1254 **Table S8**. Merged candidate list from three datasets of hyperLOPIT, ACP-BirA and
1255 APT1-TurboID. Candidates were retrieved from three datasets, and analyzed with
1256 their TMD numbers. Most listed proteins are putative transporters or proteins with high
1257 numbers of TMD.

1258 **Table S9**. Proteins identified to be in the apicoplast by epitope fusion and confocal
1259 imaging. These newly identified apicoplast proteins were listed with CRISPR scores,
1260 TMD numbers, predicted localization by HyperLOPIT, and their P. falciparum
1261 orthologues with relevant information.

1262 **Table S10**. Identification of orthologues of novel apicoplast proteins and known
1263 proteins in species belong to the chromalveolates, red algae, green algae, plants,
1264 fungi, metazoa and bacteria. The species were grouped into the taxa, and listed with
1265 their orthologues and E-values of the newly identified proteins.

1266 **Table S11**. Orthologues of AMT1 and AMT2 in selected species of apicomplexans.
1267 Orthologous were analyzed in HMMER, and accession numbers of these orthologues
1268 in the apicomplexans were listed.

1269 **Table S12**. Analysis of metabolites detected by GCMS and LCMS in the lines of TIR1,
1270 AMT1-AID, AMT2-AID and dKD induced by IAA for 18 hours. The datasets (Dataset
1271 S2) were analyzed by Dunnett's multiple comparisons.

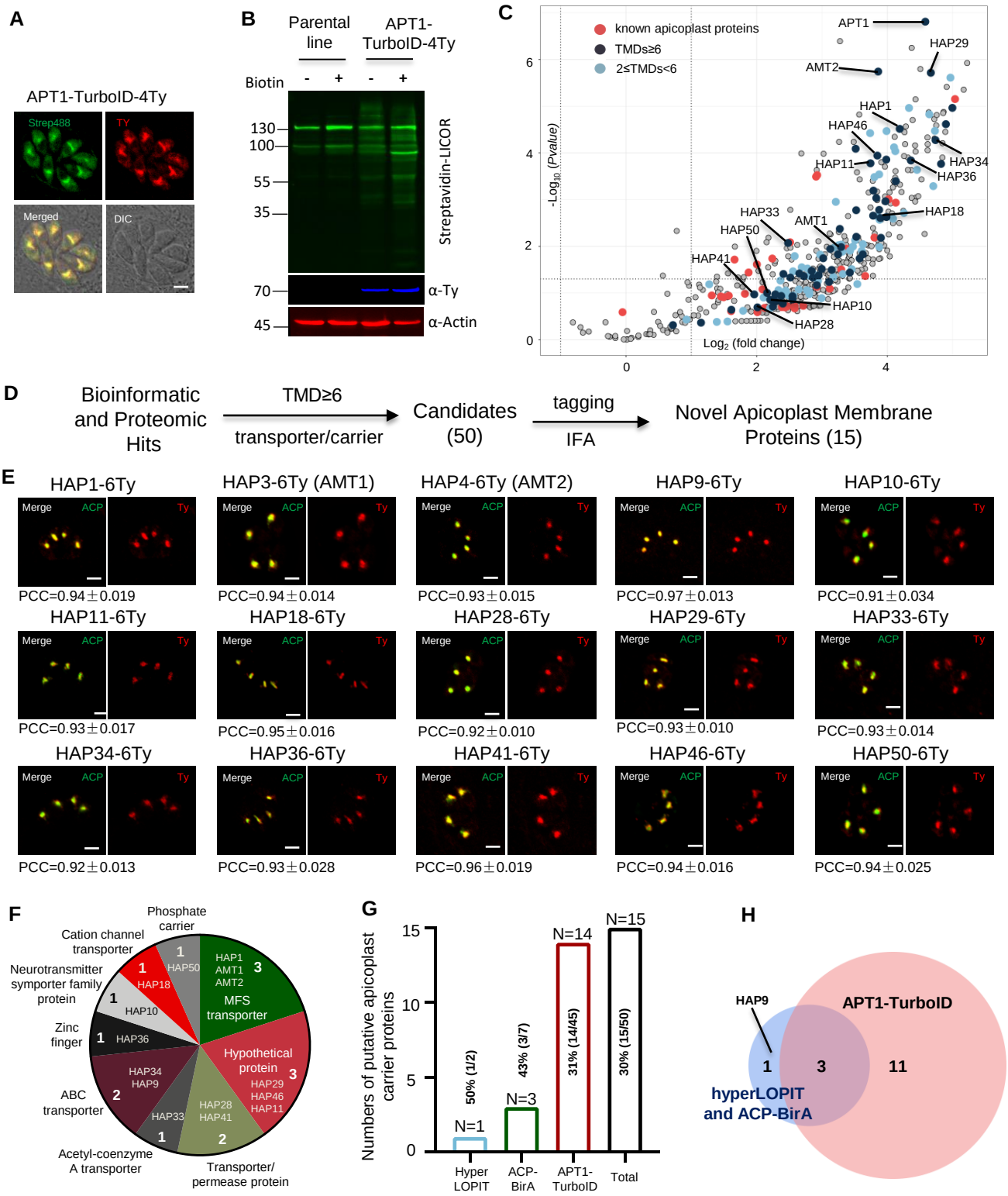
A
APT1-TurboID-4Ty
Strep488
TY
Merged
DIC
B
Parental line
APT1-TurboID-4Ty
Biotin
- + - +
130
100
55
35
70
45
Streptavidin-LICOR
α-Ty
α-Actin
C
known apicoplast proteins
TMDs≥6
2≤TMDs<6
APT1
HAP29
AMT2
HAP1
HAP46
HAP11
HAP34
HAP36
HAP18
HAP33
AMT1
HAP50
HAP41
HAP10
HAP28
-Log10 (Pvalue)
Log2 (fold change)
D
Bioinformatic and Proteomic Hits
TMD≥6
transporter/carrier
Candidates (50)
tagging
IFA
Novel Apicoplast Membrane Proteins (15)
E
HAP1-6Ty
PCC=0.94±0.019
HAP3-6Ty (AMT1)
PCC=0.94±0.014
HAP4-6Ty (AMT2)
PCC=0.93±0.015
HAP9-6Ty
PCC=0.97±0.013
HAP10-6Ty
PCC=0.91±0.034
HAP11-6Ty
PCC=0.93±0.017
HAP18-6Ty
PCC=0.95±0.016
HAP28-6Ty
PCC=0.92±0.010
HAP29-6Ty
PCC=0.93±0.010
HAP33-6Ty
PCC=0.93±0.014
HAP34-6Ty
PCC=0.92±0.013
HAP36-6Ty
PCC=0.93±0.028
HAP41-6Ty
PCC=0.96±0.019
HAP46-6Ty
PCC=0.94±0.016
HAP50-6Ty
PCC=0.94±0.025
Merge
ACP
Ty
F
Phosphate carrier
Cation channel transporter
Neurotransmitter symporter family protein
Zinc finger
ABC transporter
Acetyl-coenzyme A transporter
Transporter/ permease protein
Hypothetical protein
MFS transporter
HAP1
AMT1
AMT2
HAP50
HAP18
HAP10
HAP36
HAP34
HAP9
HAP33
HAP28
HAP41
HAP29
HAP46
HAP11
G
Numbers of putative apicoplast carrier proteins
N=1
N=3
N=14
N=15
50% (1/2)
43% (3/7)
31% (14/45)
30% (15/50)
Hyper LOPIT
ACP-BirA
APT1-TurboID
Total
H
HAP9
APT1-TurboID
1
3
11
hyperLOPIT and ACP-BirA

Figure 1

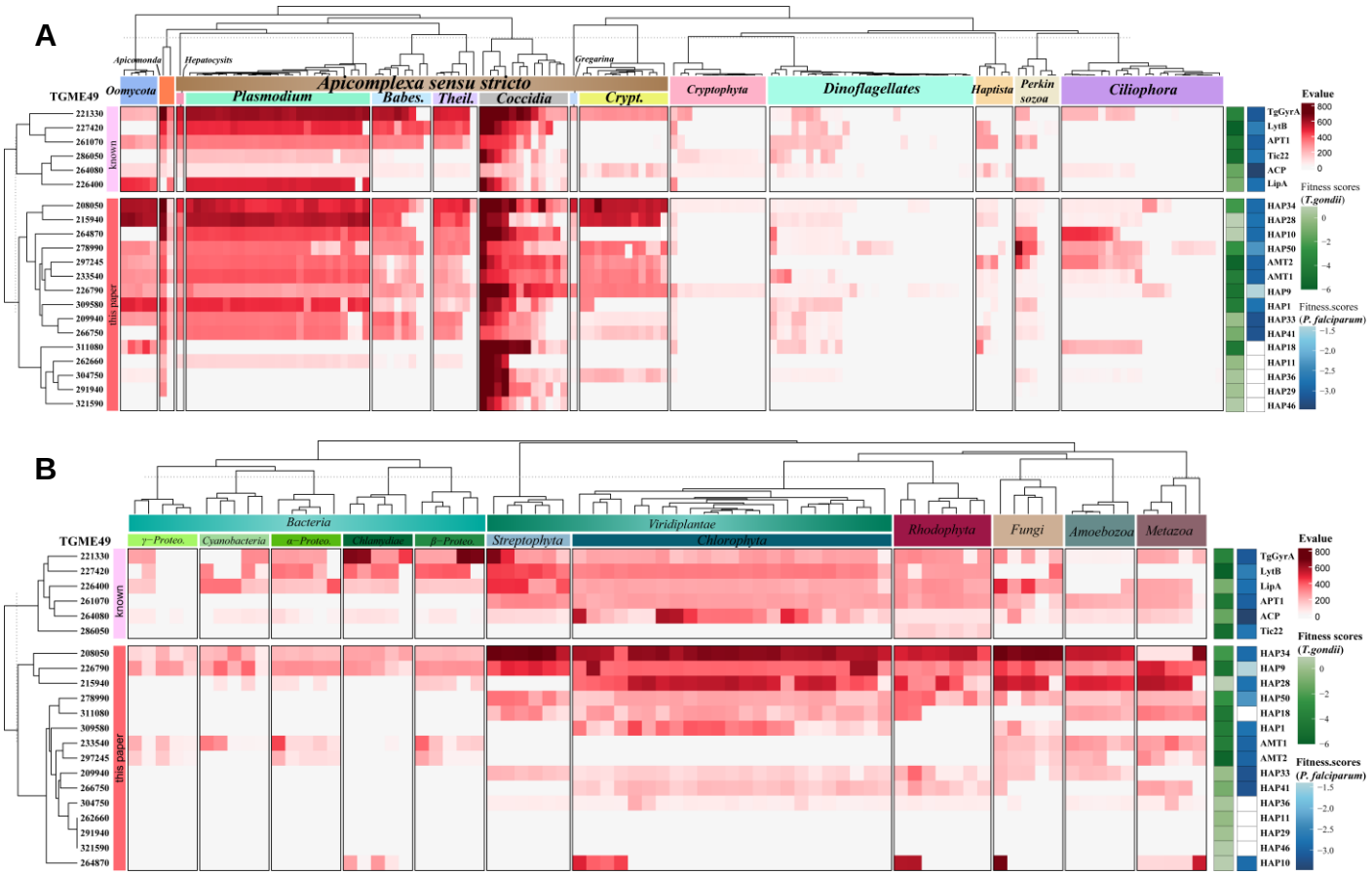
A
Apicomonda
Hepatocysits
Gregarina
TGME49
Oomycota
Apicomplexa sensu stricto
Plasmodium
Babes.
Theil.
Coccidia
Crypt.
Cryptophyta
Dinoflagellates
Haptista
Perkin sozoa
Ciliophora
221330
227420
261070
286050
264080
226400
known
208050
215940
264870
278990
297245
233540
226790
309580
209940
266750
311080
262660
304750
291940
321590
this paper
Evalue
800
600
400
200
0
TgGyrA
LytB
APT1
Tic22
ACP
LipA
Fitness scores
(T.gondii)
HAP34
HAP28
HAP10
HAP50
AMT2
AMT1
HAP9
HAP1
HAP33
HAP41
HAP18
HAP11
HAP36
HAP29
HAP46
Fitness.scores
(P. falciparum)
B
Bacteria
γ−Proteo.
Cyanobacteria
α−Proteo.
Chlamydiae
β−Proteo.
Viridiplantae
Streptophyta
Chlorophyta
Rhodophyta
Fungi
Amoebozoa
Metazoa
TGME49
221330
227420
226400
261070
264080
286050
known
208050
226790
215940
278990
311080
309580
233540
297245
209940
266750
304750
262660
291940
321590
264870
this paper
Evalue
800
600
400
200
0
TgGyrA
LytB
LipA
APT1
ACP
Tic22
Fitness scores
(T.gondii)
HAP34
HAP9
HAP28
HAP50
HAP18
HAP1
AMT1
AMT2
HAP33
HAP41
HAP36
HAP11
HAP29
HAP46
HAP10
Fitness.scores
(P. falciparum)

Figure 2

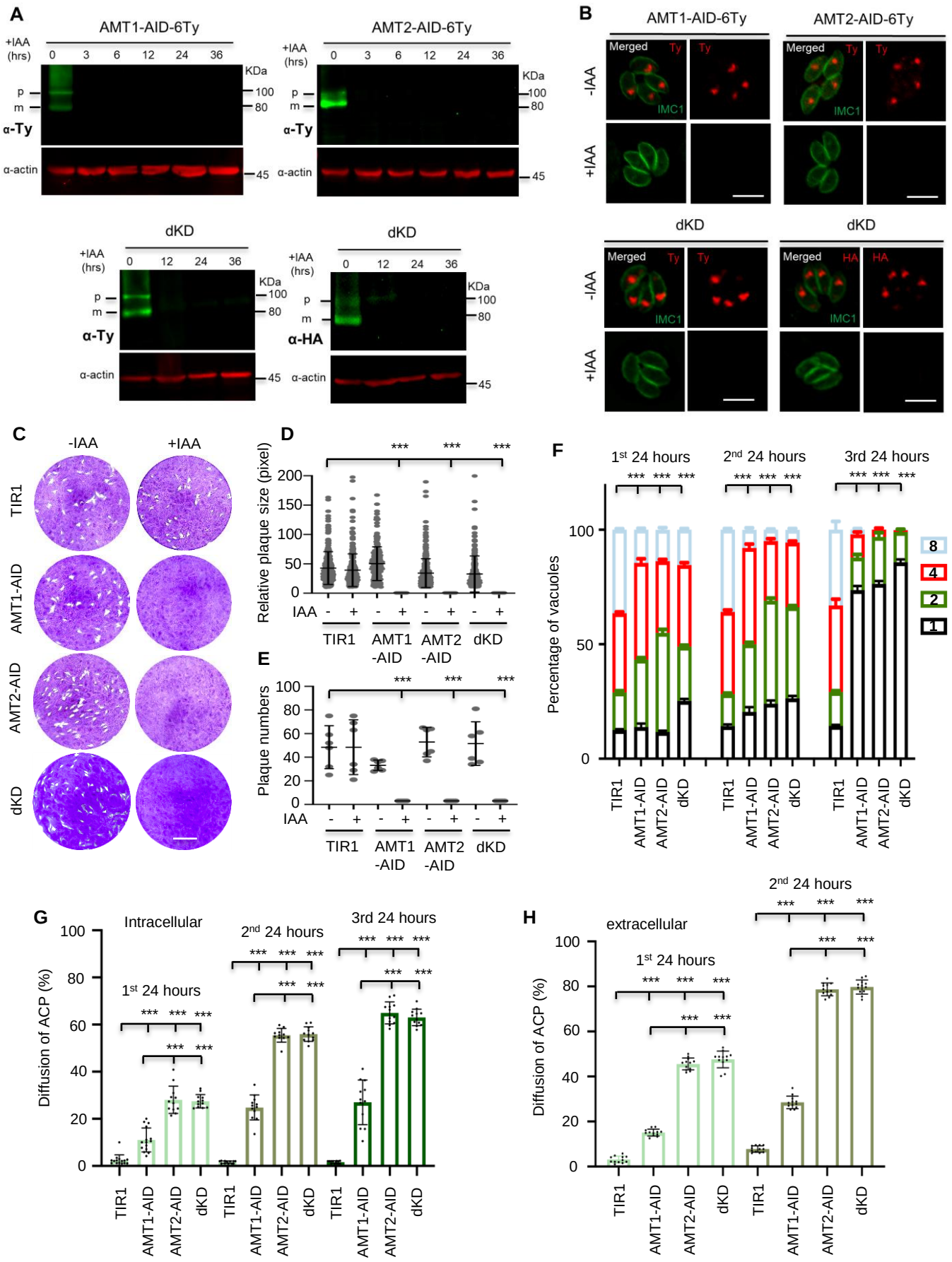
A
AMT1-AID-6Ty
AMT2-AID-6Ty
+IAA (hrs)
0 3 6 12 24 36
KDa
100
80
45
p
m
α-Ty
α-actin
dKD
0 12 24 36
α-HA
B
Merged
Ty
HA
IMC1
-IAA
+IAA
C
-IAA
+IAA
TIR1
AMT1-AID
AMT2-AID
dKD
D
Relative plaque size (pixel)
IAA
TIR1
AMT1 -AID
AMT2 -AID
dKD
E
Plaque numbers
F
1st 24 hours
2nd 24 hours
3rd 24 hours
Percentage of vacuoles
8
4
2
1
G
Intracellular
Diffusion of ACP (%)
H
extracellular

Figure 3

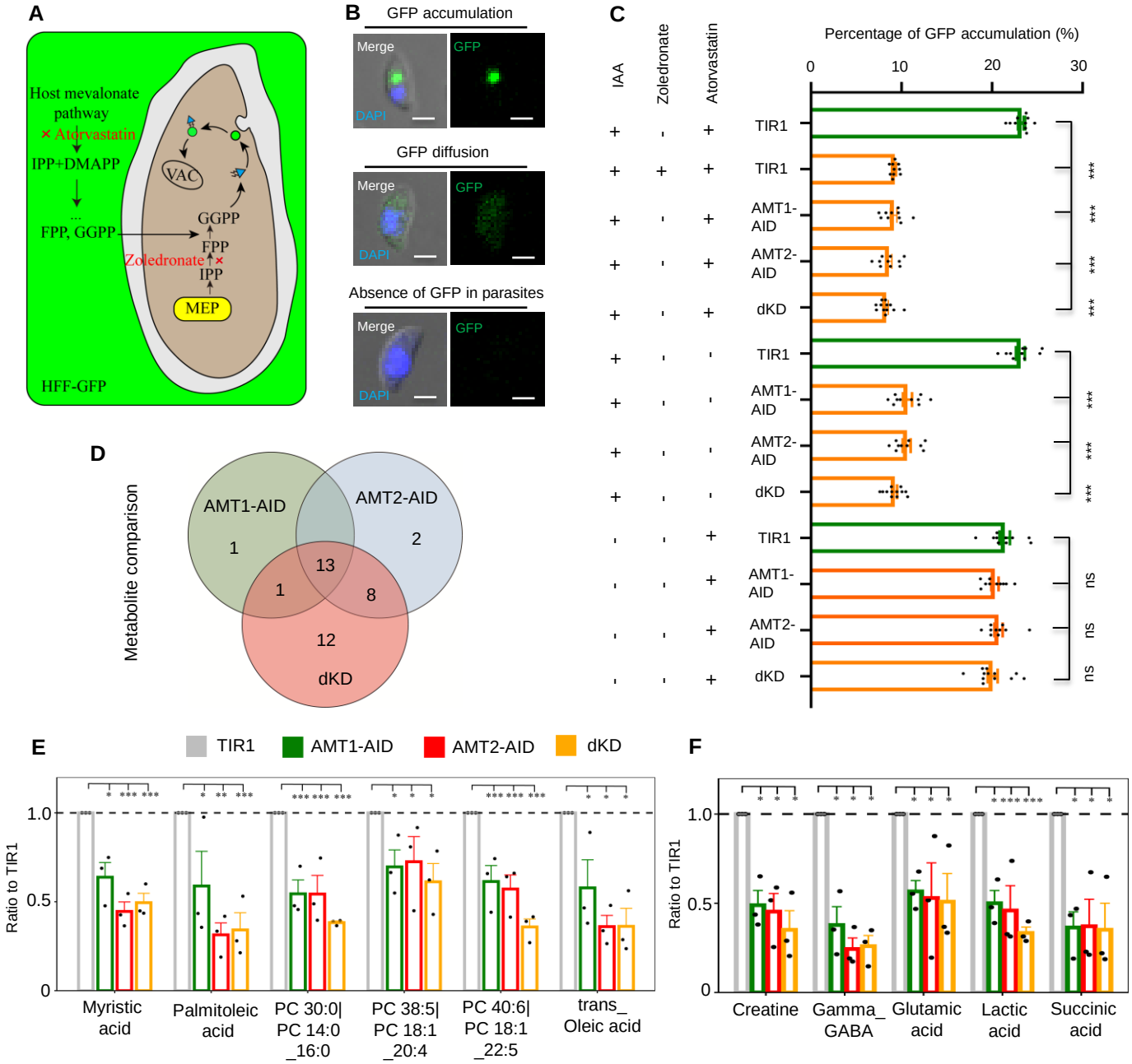
A
Host mevalonate pathway
× Atorvastatin
IPP+DMAPP
...
FPP, GGPP
VAC
GGPP
FPP
Zoledronate ×
IPP
MEP
HFF-GFP
B
GFP accumulation
Merge
GFP
DAPI
GFP diffusion
Absence of GFP in parasites
C
IAA
Zoledronate
Atorvastatin
Percentage of GFP accumulation (%)
0
10
20
30
TIR1
AMT1-AID
AMT2-AID
dKD
***
ns
D
Metabolite comparison
AMT1-AID
AMT2-AID
dKD
1
2
13
1
8
12
E
TIR1
AMT1-AID
AMT2-AID
dKD
Ratio to TIR1
1.0
0.5
0
Myristic acid
Palmitoleic acid
PC 30:0| PC 14:0 _16:0
PC 38:5| PC 18:1 _20:4
PC 40:6| PC 18:1 _22:5
trans_ Oleic acid
F
Creatine
Gamma_ GABA
Glutamic acid
Lactic acid
Succinic acid

Figure 4

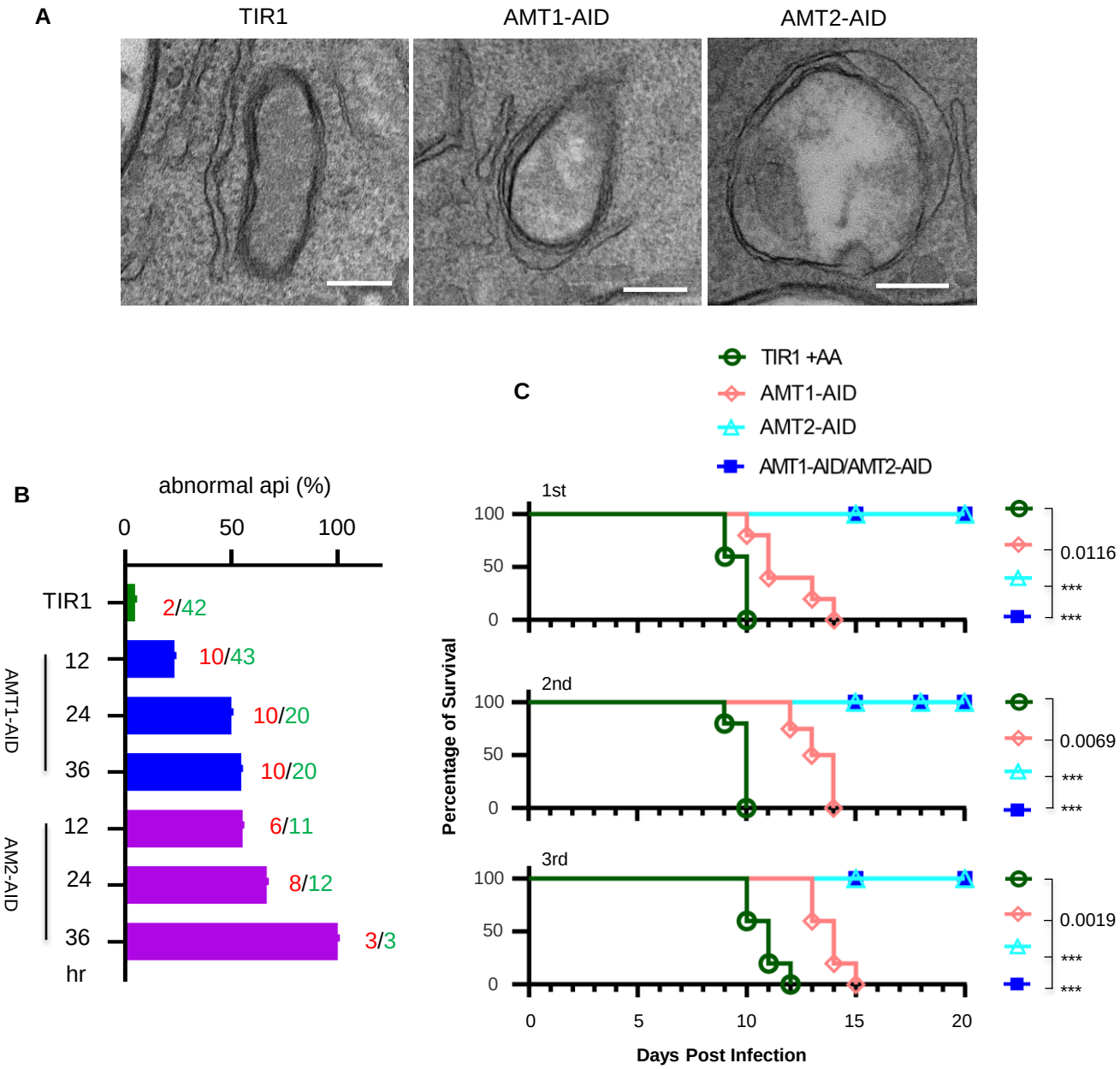
A
TIR1
AMT1-AID
AMT2-AID
B
abnormal api (%)
0
50
100
TIR1
2/42
AMT1-AID
12
10/43
24
10/20
36
10/20
AM2-AID
12
6/11
24
8/12
36
3/3
hr
C
TIR1 +AA
AMT1-AID
AMT2-AID
AMT1-AID/AMT2-AID
1st
2nd
3rd
Percentage of Survival
100
50
0
0.0116
0.0069
0.0019
***
0
5
10
15
20
Days Post Infection

Figure 5